Cell

Influenza Virus M2 Protein Mediates ESCRT-Independent Membrane Scission

Jeremy S. Rossman,[1,2] Xianghong Jing,[1,3] George P. Leser,[1] and Robert A. Lamb[1,2,*]
[1]Department of Biochemistry, Molecular Biology, and Cell Biology
[2]Howard Hughes Medical Institute
Northwestern University, Evanston, IL 60208, USA
[3]Present address: Center for Biologics Evaluation and Research, Food and Drug Administration, Bethesda, MD 20892
*Correspondence: ralamb@northwestern.edu
DOI 10.1016/j.cell.2010.08.029

SUMMARY

Many viruses utilize host ESCRT proteins for budding; however, influenza virus budding is thought to be ESCRT-independent. In this study we have found a role for the influenza virus M2 proton-selective ion channel protein in mediating virus budding. We observed that a highly conserved amphipathic helix located within the M2 cytoplasmic tail mediates a cholesterol-dependent alteration in membrane curvature. The 17 amino acid amphipathic helix is sufficient for budding into giant unilamellar vesicles, and mutation of this sequence inhibited budding of transfected M2 protein in vivo. We show that M2 localizes to the neck of budding virions and that mutation of the M2 amphipathic helix results in failure of the virus to undergo membrane scission and virion release. These data suggest that M2 mediates the final steps of budding for influenza viruses, bypassing the need for host ESCRT proteins.

INTRODUCTION

The budding of enveloped viruses is a complex multi-step process, the completion of which requires alterations in membrane curvature and scission at the neck of the budding virion. Many viruses such as HIV-1, Ebola virus and the paramyxovirus PIV-5 utilize the host endosomal sorting complex required for transport (ESCRT) machinery to mediate membrane scission and virion release (reviewed in Carlton and Martin-Serrano, 2009; Chen and Lamb, 2008). Matrix proteins from these and other viruses contain 'late' domains, sequences that bind to proteins of the ESCRT pathway, enabling the virus to utilize ESCRT proteins that are normally involved in the budding and release of endosomal vesicles into multi-vesicular bodies. However, studies indicate that influenza virus may bud independently of ESCRT proteins, utilizing an unknown mechanism of membrane scission and virion release (Bruce et al., 2009; Chen and Lamb, 2008).

Influenza virus buds from the plasma membrane of infected cells, producing both 100 nm diameter spherical and 100 nm × 2-20 μm filamentous virions. Assembly and budding is thought to begin with lipid raft-mediated clustering of the two major viral glycoproteins, the receptor binding/membrane fusion protein hemagglutinin (HA) and the enzyme neuraminidase (NA) (Chen et al., 2007; Leser and Lamb, 2005; Takeda et al., 2003). Lipid rafts are dynamic plasma membrane domains, enriched in sphingolipids and cholesterol, which are thought to serve as platforms for the concentration of proteins (Brown and Rose, 1992; Simons and Toomre, 2000). Lipid rafts are also the sites of budding for several viruses, such as influenza virus, HIV-1 and Ebola virus (reviewed in Chazal and Gerlier, 2003). Mutations in the HA transmembrane (TM) domain that eliminate association with lipid rafts, significantly attenuate viral replication and prevent the formation of filamentous virions (Chen et al., 2005).

The cytoplasmic tails of HA and NA have been inferred to bind to the matrix (M1) protein, mediating its incorporation into the budding virion (Jin et al., 1997). The M1 protein interacts with the nucleoprotein (NP) and the plasma membrane, facilitating incorporation of the genome, as a viral ribonucleoprotein complex (vRNP), into budding virions (Bui et al., 1996; Noton et al., 2007; Zhang and Lamb, 1996). Mutation of the cytoplasmic tails of HA and NA reduces the packaging of M1 and produces defective virions with greatly altered morphology (Barman et al., 2004; Jin et al., 1997). In conjunction with the HA/NA-M1 interaction, M1 binds to a third viral integral-membrane viral protein, M2. M2 is a multi-functional protein with proton-selective ion channel activity. The M1-M2 interaction may enable the recruitment of M2 to sites of virus budding and mediate the incorporation of M2 into virions (Chen et al., 2008).

M2 is an essential component of the infectious virion. During virus entry by endocytosis, endosomal acidification activates the proton selective ion channel activity of the M2 protein, causing acidification of the virus interior and leading to dissociation of M1 from the vRNP (reviewed in Lamb and Pinto, 2005; Pinto and Lamb, 2006). M2 ion channel activity is inhibited by the antiviral drug amantadine, which prevents proton flux and blocks virus uncoating by preventing M1-RNP dissociation (reviewed in Pinto and Lamb, 2007). The M2 protein contains 97 amino acid residues that assemble into a homotetramer (Pinto et al., 1997). M2 contains a 24 residue N-terminal extracellular domain, a single TM domain of 19 residues that forms the pore of the ion channel, and a 54 residue cytoplasmic tail

(Lamb and Pinto, 2005; Zebedee and Lamb, 1988; Pinto et al., 1997). The first 17 amino acid residues of the M2 protein cytoplasmic tail are predicted to form a membrane-parallel, amphipathic helix (Nguyen et al., 2008; Schnell and Chou, 2008; Tian et al., 2003). In addition to its ion channel activity, recent work has suggested that the M2 protein may also affect the morphology of budding virions and may be required for efficient vRNP packaging, assembly and budding (Chen et al., 2008; Iwatsuki-Horimoto et al., 2006; McCown and Pekosz, 2005, 2006; Rossman et al., 2010).

Whereas many of the steps required for influenza virus assembly have been determined, the molecular machinery needed to complete the budding process has not been elucidated. The available data for influenza virus indicate that the virus may bud independently of ESCRT proteins, thus the necessary components for membrane scission and virion release are not known (Bruce et al., 2009; Chen and Lamb, 2008). In this study we have identified an additional function of the M2 protein in modifying membrane curvature during virus budding. We further show that the influenza virus M2 protein mediates membrane scission, allowing for virion release independent of the host ESCRT pathway.

RESULTS

Conservation of the M2 Amphipathic Helix

Previous work has suggested that the M2 cytoplasmic tail may play a role in virus assembly (Chen et al., 2008; Iwatsuki-Horimoto et al., 2006; McCown and Pekosz, 2005, 2006; Rossman et al., 2010). Thus, we sought to elucidate the possible functions of the M2 protein during viral assembly and budding. Analysis of the M2 protein sequence predicts that the cytoplasmic tail contains an amphipathic helix, which has been confirmed experimentally (Nguyen et al., 2008; Tian et al., 2003) (Figure 1A). A helical wheel plot of the M2 amphipathic helix is shown in Figure 1B with the charged and hydrophobic faces of the helix indicated. Analysis of the amino acid sequence of M2 across all influenza subtypes for 500 different strains of influenza A virus, including the recent 2009 H1N1 pandemic strain and several highly pathogenic H5N1 avian influenza virus strains, showed significant conservation along the length of the M2 amphipathic helix (Figure S1 available online), suggesting that the amphipathic helix has an important role for influenza virus.

M2 Alters Membrane Curvature in a Cholesterol-Dependent Manner

Many proteins, including several viral proteins, utilize an amphipathic helix for modifying membrane curvature (reviewed in Antonny, 2006). To address the role of the M2 amphipathic helix in virus budding, we first assessed the effect of the amphipathic helix on membrane curvature. As M2 has been shown to bind cholesterol (Rossman et al., 2010; Schroeder et al., 2005) and cholesterol can modify the ability of an amphipathic helix to induce membrane curvature (de Meyer and Smit, 2009; Egashira et al., 2002), we also sought to address the possibility of cholesterol-dependent alterations in membrane curvature by the M2 protein.

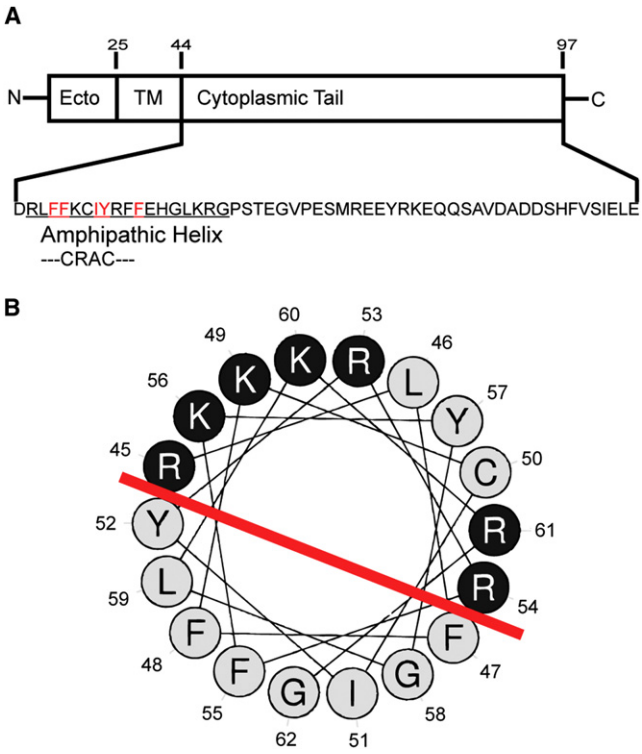

Figure 1. The M2 Amphipathic Helix

(A) Diagram of structural motifs in the M2 protein. The TM domain/ion channel pore, CRAC motif and amphipathic helix are indicated. Alanine substituted residues in the M2(AH-Mut) protein are shown in red.

(B) Helical wheel plot of the M2 amphipathic helix is shown as generated at http://heliquest.ipmc.cnrs.fr. Hydrophilic residues are shown in black and hydrophobic resides in gray. The red line separates the two faces of the helix. See also Figure S1.

Wild-type (wt) M2 protein and an amphipathic helix mutant [M2(AH-Mut)], in which the hydrophobic face of the helix was altered by changing five bulky hydrophobic residues to alanine in an attempt to disrupt the function of the helix without disrupting its α-helicity (Rossman et al., 2010), were purified and reconstituted into large unilamellar vesicles (LUVs). Examination of LUVs reconstituted with wt M2 protein by cryo-electron microscopy, or negative staining, showed an alteration in morphology from control LUVs (Figure 2A and Figure S2A). Wt M2 protein induced the formation of many 'flat' single LUVs, suggesting that M2 may induce negative membrane curvature (Chernomordik et al., 1995; Russell et al., 2001) in the presence of cholesterol (Figure 2A and Figure S2A). Additionally, changes in LUV morphology were found to be independent of M2 ion channel activity, as incubation with the ion channel blocker amantadine had no effect (Figures S2B and S2C).

Control LUVs that lacked cholesterol appeared 'flat' and resembled cholesterol-containing LUVs reconstituted in the presence of wt M2 protein (Figure 2A and Figure S2A). It has been shown that cholesterol can directly modify membrane structure, providing an explanation for the different morphology seen with control LUVs in the presence and absence of cholesterol (de Meyer and Smit, 2009). When wt M2 was reconstituted

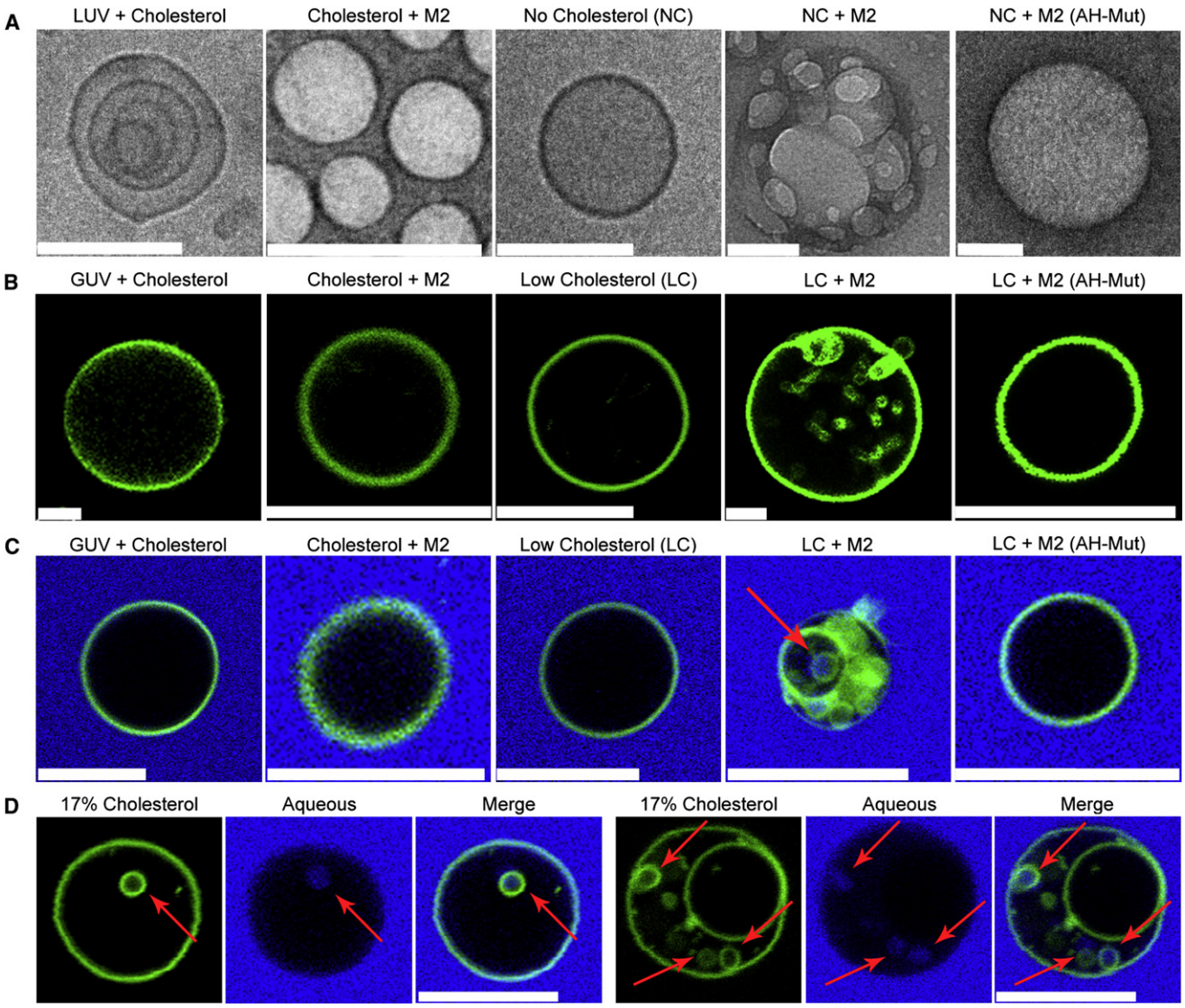

Figure 2. M2 Alters Membrane Curvature in a Cholesterol-Dependent Manner

(A) LUVs or cholesterol-free LUVs were reconstituted in the presence or absence of 100 μg purified M2 or M2(AH-Mut) protein and analyzed by cryo-electron microscopy. NC indicates LUVs containing no cholesterol. Scale bars indicate 100 nm.

(B) LUVs prepared as above, with the addition of a fluorescent membrane dye (shown in green), were dehydrated, electroformed into GUVs and immediately imaged.

(C) GUVs, prepared as above, with 50 μg purified M2 or 100 μg M2(AH-Mut) protein were resuspended with 0.5 mg/ml of lucifer yellow (shown in blue). LC indicates GUVs containing 0.5 molar % cholesterol.

(D) Two examples of M2-containing GUVs, prepared as above, containing 17 molar % cholesterol. Arrows indicate lucifer yellow containing ILVs.

The scale bars indicate 10 μm. See also Figure S2, Figure S3, and Movie S1 and Movie S2.

into LUVs that lacked cholesterol, M2 appeared to induce positive membrane curvature, and the resulting morphology resembled control LUVs that contained cholesterol (Figure 2A and Figure S2A). M2-containing LUVs that lacked cholesterol showed the formation of many small, aggregated, 'budding' LUVs that appear morphologically similar to cholesterol-containing control LUVs (Figure 2A and Figure S2A). No significant change in LUV morphology was observed when the vesicles were reconstituted with M2(AH-Mut) protein in the absence of cholesterol, suggesting that the M2 amphipathic helix is necessary for the alteration of membrane curvature in the absence of cholesterol (Figure 2A and Figure S2A).

Our previous work has shown that influenza virus expressing M2(AH-Mut) protein is not impaired in ion channel activity, protein expression or protein localization during virus infection (Ma et al., 2009; Rossman et al., 2010). However, to control for possible differences in in vitro membrane incorporation, we determined the proportion of input wt and M2(AH-Mut) mutant

M2 protein reconstituted into LUVs. Based on an input of 100 μg of wt M2 protein, it was found that 75% was incorporated into the LUVs. This amount was unaffected by the presence or absence of cholesterol; however, only 35% of M2(AH-Mut) protein was incorporated into LUVs, regardless of the presence or absence of cholesterol. To ensure that the differences in membrane curvature seen when comparing wt M2 and M2(AH-Mut) were due to the specific action of the protein, and not due to differences in protein incorporation, LUVs were made with 50 μg of wt M2 protein, which gave a final incorporated protein amount of 31 μg, which is comparable to the 35 μg level obtained with the M2(AH-Mut) protein. Examination of these LUVs showed that they retained their induction of positive and negative curvature and appeared indistinguishable from LUVs created with 100 μg of wt M2 protein (Figures S2B and S2C).

M2 Causes Membrane Budding In Vitro

As M2 is capable of altering membrane curvature, we asked if M2 protein alone is capable of causing membrane budding. We utilized a system for imaging budding and membrane scission events within giant unilamellar vesicles (GUVs) that has been described recently for analyzing the function of proteins in the ESCRT III complex (Wollert et al., 2009). GUVs were formed in the presence of 30 or 0.5 molar % of cholesterol, incorporating purified wt M2 protein or M2(AH-Mut) protein. Low-cholesterol GUVs containing wt M2 protein exhibited a rapid budding of the GUV membrane and the formation of many intra-luminal vesicles (ILVs) (Figure 2B LC+M2, Movie S1). Analysis of the ILVs showed free movement within the GUV, consistent with completion of membrane scission (Movie S1). Both inward and outward budding events were observed due to the random orientation of M2 protein in the lipid bilayer (Figure 2B); however, outward budding vesicles were seen less frequently due to rapid diffusion out of the imaging plane following membrane scission. Low-cholesterol GUVs containing M2(AH-Mut) protein resembled control GUVs (cf. Figure 2B LC and LC+M2(AH-Mut), Movie S2), suggesting that the M2 amphipathic helix is essential for M2-mediated membrane budding.

In the presence of high-levels of cholesterol, budding events were not observed for wt M2 protein (Figure 2B, Cholesterol + M2). Additionally, control GUVs showed no evidence of budding when reconstituted in the presence of high or low molar ratios of cholesterol (Figure 2B GUV + Cholesterol and LC). It is important to note that the M2-dependent induction of negative curvature seen in high-cholesterol LUVs (Figure 2A), was not observed in high-cholesterol GUVs (Figure 2B). It is possible that M2-induction of negative curvature occurs in GUVs; however, the resulting changes in morphology may not be resolvable by light microscopy and changes in vesicle size may be lost in the normal background variation of GUV size. Alternatively, the cholesterol-dependent M2-induction of negative curvature may depend on the initial degree of membrane curvature, with the different LUV and GUV radii of curvature affecting the membrane association and/or curvature induction of the M2 amphipathic helix.

M2-induced budding was confirmed via the addition of the small aqueous marker lucifer yellow to the GUV resuspension buffer. Lucifer yellow fluorescence was observed only within the intraluminal vesicles of low-cholesterol GUVs reconstituted with WT M2 protein (Figure 2C and Figure S3A). Some lucifer yellow-negative ILVs are observed, however, the M2 protein begins budding directly after GUV formation has completed and, thus, some ILVs may complete budding before the addition of lucifer yellow to the media. Additionally, to confirm that the lack of budding observed with M2(AH-Mut) seen in Figure 2B is not due to the lower protein incorporation levels, the GUVs used in Figure 2C were made from LUVs incorporating 50 μg of M2 or 100 μg of M2(AH-Mut), resulting in approximately equal incorporation of these two proteins into the vesicles. No budding was observed with the M2(AH-Mut) protein, while wt M2 appeared to bud normally (Figure 2C). As M2 is unlikely to encounter a lipid environment within the cell that is cholesterol-free, we reconstituted GUVs containing an intermediate concentration of cholesterol (17 molar %) with full-length M2 protein. In the presence of 17 molar % cholesterol, M2 caused membrane budding and the formation of lucifer yellow-containing ILVs, indicating that M2 is capable of mediating budding in physiologically-relevant levels of cholesterol (Figure 2D and Figure S3B).

To determine if the M2 amphipathic helix is sufficient to mediate GUV budding, a peptide corresponding to the M2 amphipathic helix (M2AH) was synthesized. Addition of the M2AH peptide to preformed GUVs containing 0.5 molar % of cholesterol led to rapid budding from the GUV membrane (Figure 3A, LC + Pep M2AH), resulting in 80.8% (n = 54) of the GUVs containing at least one ILV. Addition of M2AH peptide to preformed GUVs containing 30% cholesterol did not cause budding (Figure 3A cholesterol + Pep M2AH), with only 6.2% (n = 153) of the GUVs containing an ILV. As electroformed GUVs show a background level of vesicles containing ILVs [9.7% (n = 281) of low cholesterol GUVs and 3.7% (n = 42) of high cholesterol GUVs contain an ILV], we sought to determine if the ILVs observed in Figure 3A were caused specifically by peptide-induced membrane budding. Peptide-induced budding was confirmed via the addition of lucifer yellow to the GUV resuspension buffer. Addition of lucifer yellow to the GUV resuspension buffer lead to fluorescence only within low-cholesterol GUVs that had been treated with the M2AH peptide [72.5% (n = 54) of peptide treated low cholesterol GUVs contained a lucifer yellow positive ILV, compared to 3.5% (n = 281) without peptide and 0.5% (n = 153) for peptide-treated high cholesterol GUVs; Figure S3c], thus confirming that the M2 amphipathic helix is capable of inducing budding and the uptake of surrounding aqueous media into ILVs (Figure 3B, LC + Pep M2AH). Interestingly, addition of the M2AH peptide to low-cholesterol GUVs appeared to cause membrane leakage, in addition to membrane budding, as shown by the presence of aqueous lucifer yellow marker within the bulk GUV interior, as well as within the budded intra-luminal vesicles (Figure 3B). It is possible that the M2AH peptide possess the ability to form pores in the membrane bilayer, such as has been noted for several other amphipathic peptides (Egashira et al., 2002; Lamaziere et al., 2007; Lee et al., 2008). Pore formation leading to membrane leakage is seen with the class-A amphipathic peptide Ac-18A-NH2 (Venkatachalapathi et al., 1993) and pore formation leading to GUV lysis is seen with the class-L

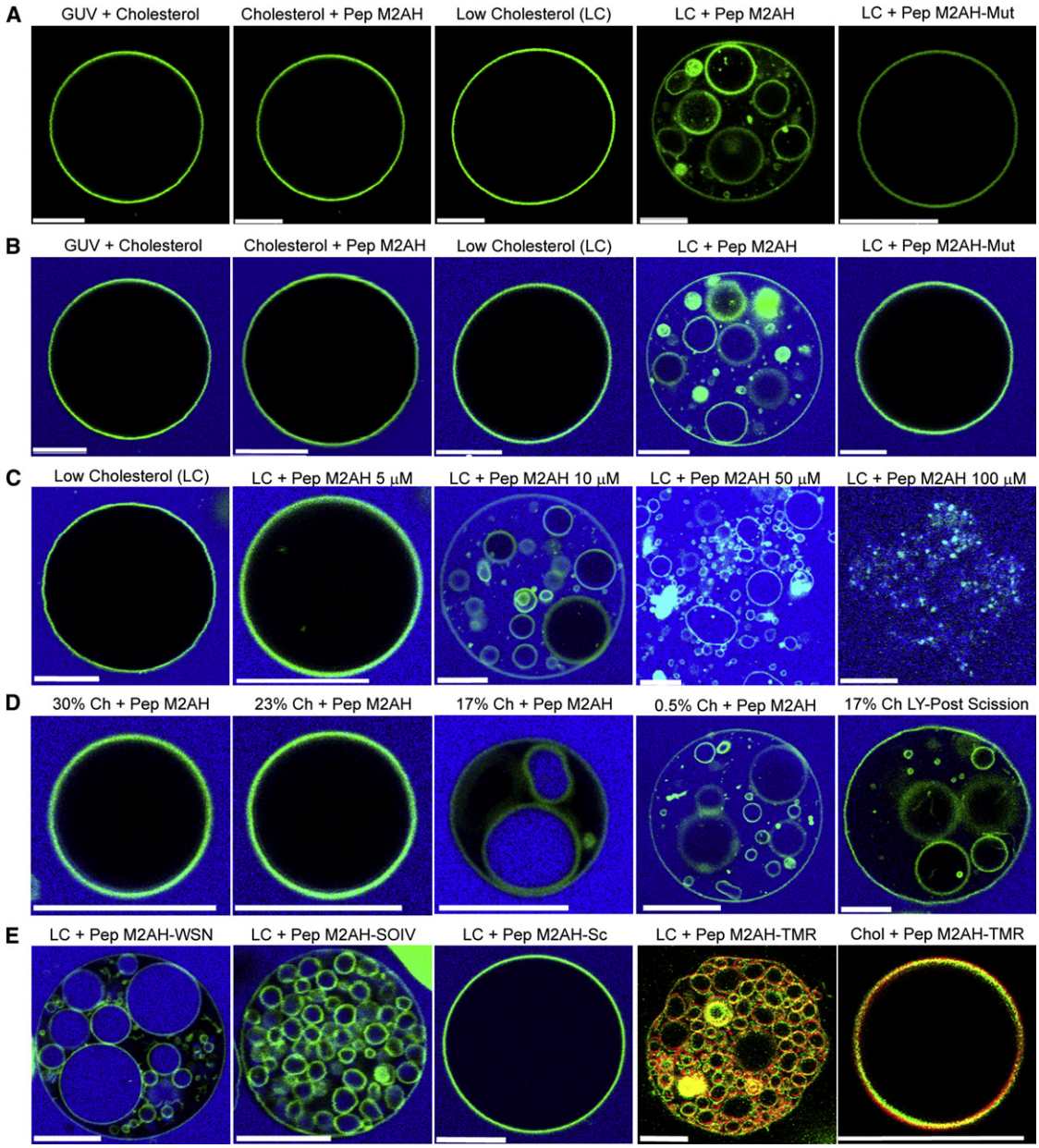

Figure 3. The M2 Amphipathic Helix Causes Membrane Budding In Vitro

(A) GUVs electroformed with 30 or 0.5 molar % of cholesterol were treated with 10 μM of the indicated peptide and imaged within 1 hr.

(B) GUVs were prepared and treated as above except that 0.5 mg/ml of lucifer yellow (shown in blue) was added to the resuspension buffer.

(C) GUVs, prepared as above, were treated with M2AH peptide at the indicated concentrations for 1 hr and imaged.

(D) GUVs, prepared as above with the indicated molar % of cholesterol, were treated with 10 μM of M2AH peptide for 1 hr and imaged. 17% cholesterol LY-post scission indicates 17% cholesterol GUVs to which lucifer yellow was added 1 hr post-treatment with 10 μM of M2AH peptide.

(E) GUVs, prepared as above (with the exception of M2AH-TMR treated samples, for which lucifer yellow was omitted from the resuspension buffer), were treated with 10 μM of the indicated peptide and imaged within 1 hr. The M2AH-WSN peptide corresponds to the M2 amphipathic helix of A/WSN/33, M2AH-SOIV to A/California/05/2009, M2AH-Sc to a scrambled sequence of the M2AH peptide, M2AH-TMR to rhodamine-labled M2AH peptide. LC indicates GUVs containing 0.5 molar % of cholesterol.

The scale bars indicate 10 μm. See also Figure S3, Figure S4, and Movie S3.

amphipathic peptide melittin (reviewed in Dempsey, 1990) (Figure S4). However, in the context of the intact M2 protein, it is likely that the transmembrane domain and the full cytoplasmic tail limits the ability of the amphipathic helix to transverse the bilayer as shown by the absence of membrane leakage during M2 GUV budding (Figures 2C and 2D).

Titration of the peptide concentration required to induce budding showed no effect at 5 μM, robust inward budding at 10 μM, a switch to outward budding causing GUV deformation at 50 μM and robust outward budding leading to lysis of the GUV at 100 μM (Figure 3C and Movie S3), indicating a dose-dependent alteration in membrane curvature. The ability of amphipathic helices to modify membrane curvature and cause budding is well established (reviewed in Drin and Antonny, 2010) and is shown for the amphipathic peptide RW16 (Lamaziere et al., 2007) (Figure S4). Additionally, several amphipathic helices have been shown to induce both inward and outward budding depending on the peptide concentration (Lamaziere et al., 2007), possibly due to concentration-dependent shifts in peptide orientation in the membrane. A similar activity may occur with the M2 amphipathic helix peptide, causing the different forms of budding and membrane leakage observed in Figure 3C.

Because full-length M2 protein is capable of causing budding in the presence of intermediate levels of cholesterol, we titrated the amount of cholesterol that was required to enable GUV budding by the M2AH peptide. The M2AH peptide induced GUV budding at cholesterol levels at and below 17 molar % (Figure 3D), a level that is likely comparable to many regions of the bulk plasma membrane and is consistent with the cholesterol-dependence of the full-length M2 protein. Interestingly, treatment of GUVs, containing 17 molar % cholesterol, with the M2AH peptide caused budding without membrane leakage (Figure 3D); further suggesting that the membrane leakage observed in Figure 3B is not relevant to the budding activity of the M2 protein. To further confirm the completion of M2-mediated scission, GUVs containing 17 molar % of cholesterol were treated with the M2AH peptide for 1 hr and then lucifer yellow was added to the imaging buffer. Lucifer yellow was not found in the GUV or the ILVs, indicating that the majority of ILVs had completed scission within the 1 hr treatment and were no longer assessable to the outside buffer (Figure 3D, 17% Ch LY-Post Scission).

A synthetic peptide corresponding to the amino acid sequence of the M2(AH-Mut) amphipathic helix did not cause GUV budding in the presence of low-levels of cholesterol (Figures 3A and 3B, LC + Pep M2AH-Mut), nor did a peptide containing a scrambled version of the M2AH peptide sequence (Figure 3E, LC + Pep M2AH-Sc). M2AH peptide-induced budding was further confirmed by the observation that a fluorescently-labeled version of the M2AH peptide colocalized with budded ILVs in low-cholesterol GUVs (Figure 3E, LC + Pep M2AH-TMR) and with the GUV membrane in the presence of high-cholesterol levels (Figure 3E, Chol + Pep M2AH-TMR). Additionally, treatment of low-cholesterol GUVs with peptides corresponding to the M2 amphipathic helix of the influenza virus strain A/WSN/33 or of the consensus sequence for the 2009 H1N1 pandemic swine-origin influenza virus (SOIV) strain lead to a rapid budding of the GUV membrane (Figure 3E, LC + Pep M2AH-WSN and LC + Pep M2AH-SOIV). The M2AH peptides exhibited a slight variation in their effects, with the M2AH-WSN peptide showing reduced membrane leakage and the M2AH-TMR peptide showing enhanced GUV lysis at the 10 μM concentration used. However, the consistent induction of membrane budding in a low-cholesterol environment suggests that M2-mediated membrane budding is a highly conserved function of the M2 protein.

M2 Causes Budding at Lipid Phase Boundaries

As the M2 protein is capable of inducing budding from single-phase GUVs, we asked if M2 could mediate budding from a phase-separated GUV that may better mimic domains within the plasma membrane (Kaiser et al., 2009). GUVs containing sphingomyelin, poly-unsaturated phosphocholine and cholesterol segregate into lipid ordered (Lo) and lipid disordered (Ld) phases. Incorporation of fluorescent markers allows visualization of the two phases (Figure 4A). Addition of a fluorescently-tagged M2AH peptide to phase-separated GUVs showed that the amphipathic helix binds to the Ld phase and clusters at the phase boundary (Figure 4B). Treatment of high-cholesterol GUVs with the M2 amphipathic helix peptide did not cause budding and had no observable effect on lipid phase separation (Figure 4C). However, M2AH peptide-treatment of low-cholesterol phase-separated GUVs lead to rapid outward budding beginning with the excision of the Lo phase from the GUV, in a manner that may be similar to the scission and release of the lipid-raft rich budding virus from the bulk-phase plasma membrane, and resulting in numerous, smaller, single-phase vesicles (Figures 4D and 4E, Figure S5A, and Movie S4). This suggests that the M2 amphipathic helix may modify the line tension between lipid phases, subsequently driving budding as has been previously observed for other proteins that mediate budding and scission (Allain and Ben Amar, 2006; Liu et al., 2006; Romer et al., 2010).

To confirm that the full-length M2 protein similarly localizes to the Ld phase we created plasma membrane spheres (Lingwood et al., 2008) from M2 and M2 (AH-Mut) expressing cells. By crosslinking GM1 and using immunofluorescence staining to detect M2, we observed segregation of the Lo phase and M2, suggesting that M2 is localized to the Ld phase in living cells (Figure 4F). Additionally, budding Lo vesicles were seen at the phase boundary between Lo and M2 with cells expressing wt M2 but not the mutant M2 (AH-Mut) (Figure 4G and Figures S5B and S5C), further suggesting that while the M2 amphipathic helix does not appear to be necessary for the localization of M2 to the Ld phase, the modulation of line tension causing Lo phase budding requires the wt M2 amphipathic helix.

M2 Causes Membrane Budding In Vivo

As the M2 amphipathic helix is sufficient to induce budding in an in vitro liposome assay, we assessed the ability of the M2 protein to induce budding in vivo. Transfection of an M2 expression plasmid into 293T cells led to the budding and release of M2-containing vesicles that could be detected by immunoblotting (Figure 5A) and by electron microscopy (Figure 5B). Wt M2 vesicles appeared aggregated; however, it is unlikely that this reflects any biologically-relevant activity, as aggregation may have occurred during concentration of the vesicle-containing supernatant prior to imaging. The release of M2-containing vesicles into the culture supernatant was dependent on an intact amphipathic helix, as expression of M2(AH-Mut) in 293T cells led to a significant reduction in M2 vesicle release, even when accounting for the reduced expression level as compared to

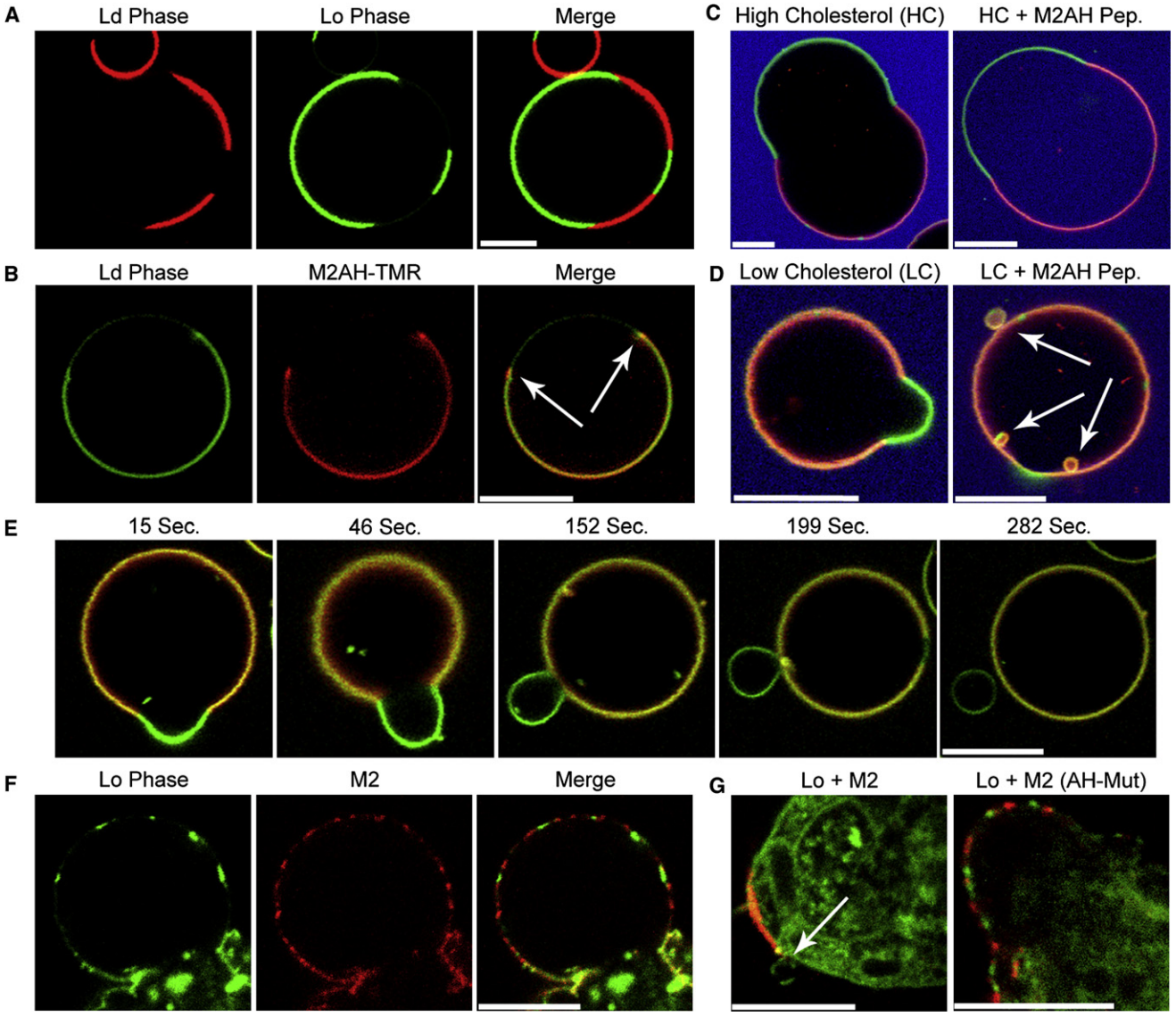

Figure 4. The M2 Amphipathic Helix Causes Membrane Budding at Phase Boundaries

Phase-separated GUVs, electroformed with 20 or 5 molar % of cholesterol and fluorescent markers for the Lo and Ld phase, were treated as indicated and imaged within 1 hr.

(A) Representative example of phase-separated GUV containing 20 molar % of cholesterol.

(B) Phase-separated GUVs were prepared as above with the Lo marker omitted. GUVs were treated with 10 μM of the M2AH-TMR peptide for 1 hr and imaged. Arrows indicate clustered M2AH peptide at the phase boundary.

(C and D) (C) Phase-separated GUVs prepared as in Figure 4A containing 20 molar % cholesterol or (D) 5 molar % were resuspended with lucifer yellow, treated with 10 μM of the M2AH peptide for 1 hr and imaged. Ld phase is shown in red, the Lo phase in green and the aqueous media in blue.

(E) Time lapse images of a GUV from Figure 4D. Note: loss of the Ld signal in later time points is due to the rapid bleaching of the red signal.

(F and G) (F) Plasma membrane spheres were prepared from wt M2 expressing cells or (G) M2(AH-Mut) expressing cells, GM1 was crosslinked to mark the Lo phase (green) and spheres were stained for M2 (red).

The scale bars indicate 10 μm. Arrows indicate sites of budding. See also Figure S5 and Movie S4.

wt M2 (Figure 5). We have shown previously that M2 exhibits only minimal cholesterol binding when expressed in the absence of other viral proteins (Rossman et al., 2010). Thus, M2 expressed by transient transfection may mediate in vivo budding from lower-cholesterol regions of the plasma membrane in a manner that is dependent on the amphipathic helix, similar to the in vitro budding of M2 from low-cholesterol GUVs (Figure 2, Figure 3, and Figure 4).

M2 Localization at the Point of Membrane Scission

For M2 to mediate membrane scission in virus-infected cells, the M2 protein needs to localize specifically to the neck of the

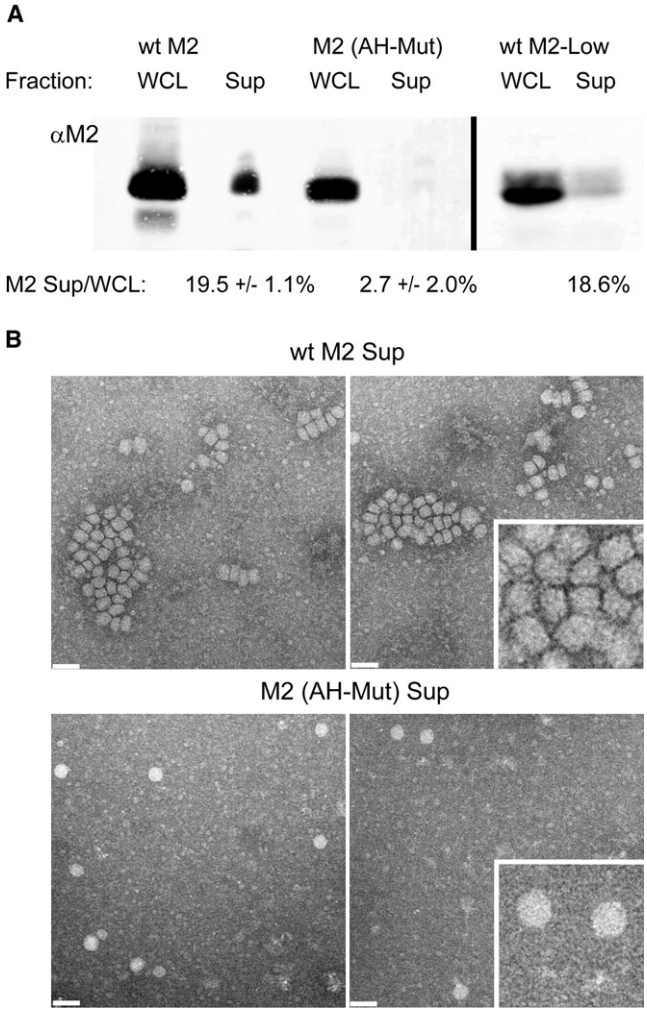

Figure 5. M2 Causes Membrane Budding In Vivo

(A) 293T cells were transfected with M2 or M2(AH-Mut) expression plasmids and 24 hr post-transfection the supernatant was harvested, concentrated, and M2 content was analyzed by Western blot as compared to whole cell lysates. Values indicate average ± standard deviation of the percentage of M2 found in the supernatant and calculated from a minimum of three repeats. M2-low indicates cells transfected with a 4-fold reduction of DNA to provide comparable M2 expression levels to that of M2(AH-Mut). The vertical line indicates separate blots.

(B) Concentrated supernatant from Figure 5A was analyzed by electron microscopy. Scale bars indicate 100 nm. The inset is an enlargement of a 100nm square region of the panel below.

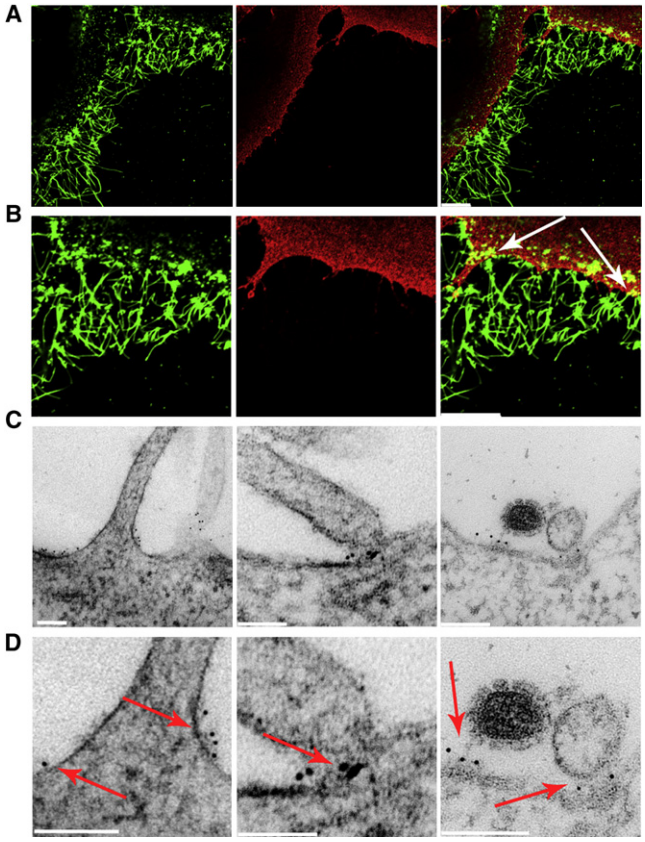

Figure 6. M2 Localizes to the Neck of Budding Virions

MDCK cells were infected with an MOI of 3 pfu/cell of A/Udorn/72 for 18 hr.

(A) Virus-infected cells were fixed and processed for immunofluorescent detection of HA (shown in green) and M2 (shown in red).

(B) Magnification of images shown in Figure 6A. The scale bars indicate 10 μm.

(C) Virus-infected cells were stained for M2 via immuno-gold labeling and thin sections were analyzed by electron microscopy.

(D) Magnification of images shown in Figure 6c.

The scale bars indicate 100 nm. Arrows indicate M2 foci at sites of virus budding. See also Figure S6.

budding virion. We have shown previously that M2 is recruited to lipid rafts and to sites of budding during virus infection (Rossman et al., 2010). However, whereas M2 can be generally localized to the base of budding filamentous virions (Figures 6A and 6B), the specific localization of M2 cannot be resolved via light microscopy. Thus, we examined the localization of M2 in virus-infected cells by immuno-gold labeling and electron microscopy. We observed that M2 localized to the base of budding filamentous and spherical virions, and a specific localization at the neck of budding viruses could be seen for 59.9% (n = 1038) of all immunogold-labeled M2 (Figures 6C and 6D), confirming our previous results showing that the majority of M2 in virally-infected cells is found at sites of virus budding (Rossman et al., 2010).

M2 localization predominantly but not exclusively to the base of virions was also observed on viral filaments that had completed the budding process. Using fluorescent microscopy, it was observed that in a population of filamentous and spherical virions M2 is concentrated at one end of the filamentous particles (Figure S6a). Quantification showed that 63% of filaments (n = 300) had a detectable focus of M2, representing the majority of M2 in the virus. Electron microscopy studies show that one end of filamentous and a focus on spherical virions reacts with antibody to M2 and accounts for 79.8% (n = 213) of all immunogold-labeled M2 found on the virion (Figure S6b). This concentration of M2 is not seen at the free end of budding viral filaments, but instead colocalizes with the site of budding (Figure 6), suggesting that M2 is incorporated during the completion of budding, at the trailing end of filamentous virions. This is

consistent with the role of M2 in mediating membrane scission and virion release.

Recent results have shown that influenza virus budding is dependent on the expression of Rab11 (Bruce et al., 2010). Rab11 is known to function in endosomal budding as well as trafficking of proteins to the apical plasma membrane, thus knock-down of Rab11 could have a direct role in membrane scission or could affect the transport of influenza virus proteins, such as M2. siRNA knock-down of Rab11a/b led to greater than 85% knock-down in Rab11a protein levels (Figure S7A) and a statistically-significant 40% reduction in the levels of M2 found on the cell surface, while the levels of HA increased 2-fold (Figures S7B and S7C). This difference cannot be attributed to expression differences as the levels of HA and M2 were comparable in control and Rab11 knock-down cells (Figure S7D). Thus, while a further affect of Rab11 cannot be ruled out, it is likely that Rab11 has an essential role in the transport of M2 to the apical membrane and not a direct role in membrane scission.

Mutation of the M2 Amphipathic Helix Blocks Membrane Scission

Although the data shown here indicate that M2 localizes to the neck of budding viruses and is capable of mediating budding and membrane scission in vitro as well as in vivo, it does not distinguish between an additive role of the M2 protein in virus budding and a necessary role for the M2 protein in mediating membrane scission. To determine whether the M2 amphipathic helix is required for virus budding and membrane scission, we examined the budding of wt and M2 mutant influenza viruses by thin section electron microscopy. Whereas in wt virus-infected cells the budding of filamentous and spherical virions could be observed at the cell surface (Figure 7A), cells infected with M2(AH-Mut) virus showed the presence of many virions in the process of budding; however, the scission and release of these virions appeared to be impaired (Figures 7A and 7B). These mutant virions on the surface of M2(AH-Mut) virus-infected cells exhibited the classical "beads on a string" morphology found in viruses with late domain mutations that are unable to recruit host ESCRT proteins, and so fail to undergo membrane scission (Figure 7B) (Yuan et al., 2000). It is important to note that, though the membrane neck connecting each of the attached virions was not always visible, this is most likely due to its presence out of the plane of sectioning. Immuno-gold labeling of M2(AH-Mut) incompletely-budded virions showed that 56.5% (n = 929) of all gold particles localized to M2 foci at the base of the budding M2(AH-Mut) virions and also at the constrictions between incompletely budded virions (Figure 7C). This suggests that M2 is incorporated into the virion as budding nears completion and that mutation of the M2 amphipathic helix leads to incorporation of M2 at the membrane proximal end of each particle; however, M2 is unable to complete membrane scission, resulting in a string of attached particles. The 'beads on a string' morphology is also found during infection with a virus that does not produce the M2 protein (ΔM2; Figures 7A and 7D), confirming an earlier observation (McCown and Pekosz, 2006). The failed-scission morphology of both M2(AH-Mut) and ΔM2 viruses (Figures 7B and 7D), coupled with previous results showing that these viruses have a significant growth defect and are impaired in viral particle release (Cheung et al., 2005; Jackson and Lamb, 2008; Rossman et al., 2010), suggests that M2 plays a necessary role in mediating membrane scission and is required for the efficient release of budding virions.

DISCUSSION

Although many steps in the assembly of influenza virus have been proposed, the final pinching off of a budding virion (membrane scission) lacks for a mechanistic explanation. In this study we identify a crucial role for the influenza virus M2 protein in virus budding. We observe that M2 is capable of altering membrane curvature, causing membrane budding and scission in a reduced-cholesterol environment (Figure 2). During virus assembly and budding, M2 localizes to the neck of budding virions (Figure 6) where it is required for membrane scission and the release of budding virions (Figure 7).

Our previous work showed that expression of HA, NA or M2 causes budding in a VLP system, however, expression of both HA and M2 increased the efficiency of VLP release compared to each protein alone (Chen et al., 2007). During virus infection, mutation or deletion of HA eliminates the production of infectious virus, but does not significantly alter the numbers of viral particles that bud from the cell (Chen et al., 2005; Pattnaik et al., 1986). In contrast, mutation or deletion of the M2 protein impairs both infectivity as well as viral particle release, for multiple different influenza virus strains (Chen et al., 2008; Cheung et al., 2005; Iwatsuki-Horimoto et al., 2006; McCown and Pekosz, 2005, 2006; Rossman et al., 2010). In the absence of M2, budding virions still form, however, membrane scission and virion release never occurs (Figures 7B and 7D). This suggests that HA may be able to initiate the budding event, but that assembly of other viral proteins may prevent membrane scission until the recruitment of M2.

Following the HA-mediated initiation of virus budding, M1 may bridge HA and M2, allowing for the recruitment of M2 to the, lipid-raft enriched, sites of virus budding (Chen et al., 2008; Rossman et al., 2010). M2 in this cholesterol-rich environment would be unable to induce membrane scission (Figure 2) and may induce negative membrane curvature instead (Figure 2A). This block in scission may stabilize the site of virus budding long enough to allow for recruitment and assembly of the full complement of viral proteins. Virion assembly may eventually deplete the local pool of raft-associated HA, placing M2 at the boundary between the lipid ordered phase of the budding virus and the lipid disordered phase of the bulk plasma membrane (Rossman et al., 2010). Acting at the phase boundary, insertion of the M2 amphipathic helix into the Ld phase may alter the line tension between the lipid phases (Figure 4). M2-mediated modifications of line tension may provide the driving force for alterations in membrane curvature, as has been previously suggested for other line-tension altering proteins (Allain and Ben Amar, 2006; Liu et al., 2006; Romer et al., 2010). Alternatively, the M2 amphipathic helix may only be able to insert into low-cholesterol membranes due to rigidifying effects of cholesterol. Deep insertion of the amphipathic helix into the membrane may directly induce lipid packing defects, causing alterations in membrane curvature without the need for line tension-derived energy. Alteration of membrane

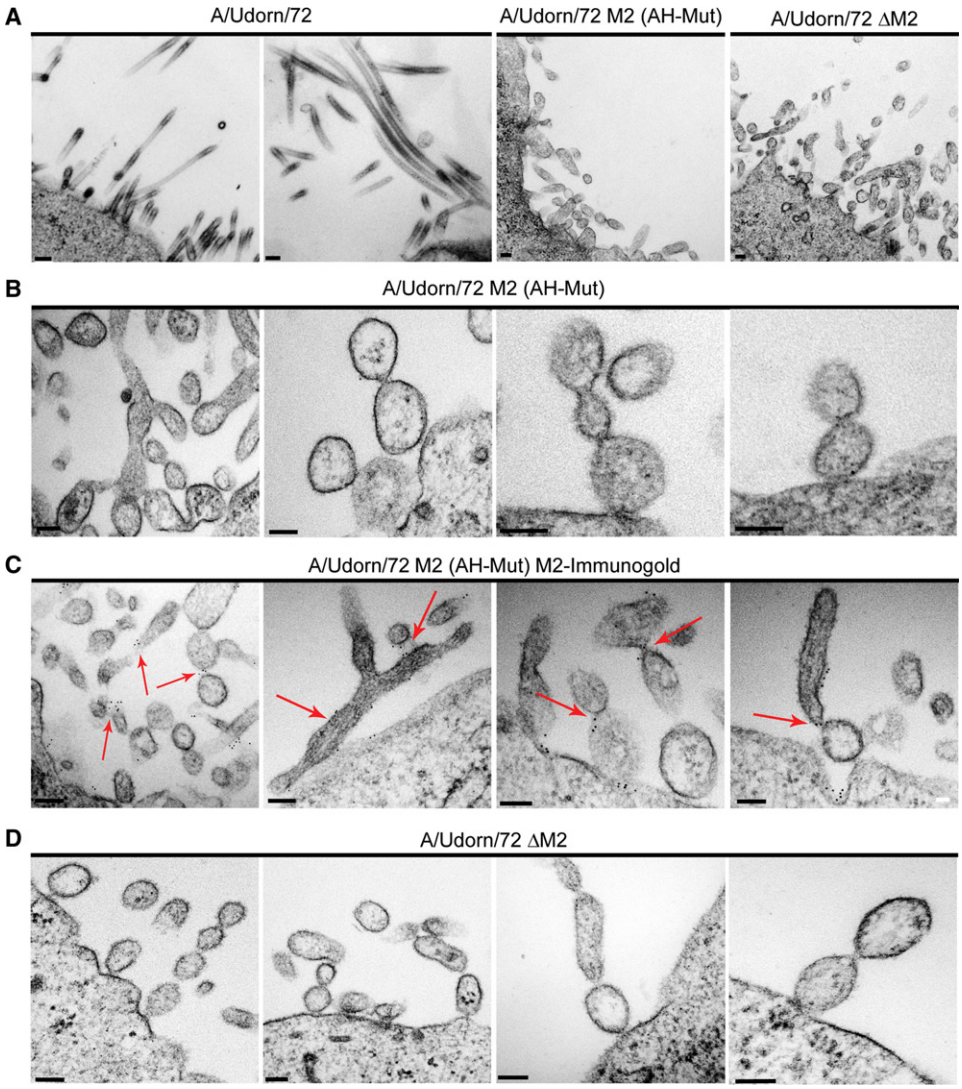

Figure 7. The M2 Amphipathic Helix is Necessary for Membrane Scission and Virion Release

MDCK cells were infected with an MOI of 3 pfu/cell of (A) A/Udorn/72, (A–C) A/Udorn/72 M2(AH-Mut) or (D) A/Udorn/72-ΔM2 for 18 hr and thin sections were analyzed by electron microscopy. M2 was detected via immunogold labeling in (C). Arrows indicate foci of M2 at points of failed membrane scission. The scale bars indicate 100 nm.

curvature at the neck of the budding virus may be sufficient to cause membrane scission and the release of the budding virus (Figure 2, Figure 3, Figure 6, and Figure 7). Mutation of the M2 amphipathic helix or alteration of M2 localization though disruption of M1 binding prevents membrane scission and the release of the budding virion, explaining the growth defect observed in both mutant viruses (Chen et al., 2008; McCown and Pekosz, 2006; Rossman et al., 2010).

Our results show a mechanism for influenza virus budding, that of a virus-encoded scission machine. Future investigation will determine if other enveloped viruses whose budding is thought to be ESCRT-independent (reviewed in Chen and Lamb, 2008) also encode their own ESCRT-substitutes, capable of mediating membrane scission and virus release. Our data show that the M2 amphipathic helix is necessary and sufficient to mediate membrane scission, and suggest that M2 may function as a virus-encoded ESCRT substitute, responsible for mediating the budding of influenza virions. Thus, we conclude that M2 is a multifunctional protein that, in addition to its proton-selective ion channel activity, has an essential role in virus budding.

EXPERIMENTAL PROCEDURES

Cell, Viruses, and Reagents

Madin-Darby canine kidney (MDCK) cells, M2-MDCK cells, 293T cells, viral stock propagation and viral infections were as previously described (Chen et al., 2008). M2 AH-Mut (previously called M2-Helix) and ΔM2 recombinant viruses have been previously described (Rossman et al., 2010; Jackson and Lamb, 2008). Antibodies used were: αHA (NR3118, BEI, Manassas, VA) and

αM2 (ectodomain mAb 14C2; (Zebedee and Lamb, 1988). Peptides were synthesized by GenScript (Piscataway, NJ). Additional detail is included as supplemental information.

Immunofluorescence Microscopy

MDCK cells grown on glass coverslips were infected as indicated, fixed and stained for HA and M2. Virus supernatant was stained following spotting on a glass coverslip. For Rab11 knock-down, A549 cells were transfected with control siRNA or siRNAs targeting Rab11a and Rab11b, infected as indicated and stained for HA and M2. Fluorescent intensity was quantified for 50–100 cells and averaged. Images were collected on a LSM5 Pascal (Zeiss, Thornwood, NY) confocal microscope.

Electron Microscopy

LUVs were treated as indicated and stained with phosphotungstic acid before imaging. For cryo-electron microscopy, LUVs were imbedded in vitreous ice using an FEI Vitrobot (Hillsboro, Or) and imaged using a Gatan (Pleasanton, CA) cryo-holder. For analysis of virus-infected cells, MDCK cells were treated as indicated and subjected to preembedding αM2 immunogold labeling followed by thin section examination as previously described (Leser et al., 1996). Samples were imaged on a JEOL 1230 (Tokyo, Japan) electron microscope.

Protein Purification

M2 and M2(AH-Mut) were expressed using the Bac-N-Blue baculovirus expression system (Invitrogen) and purified as previously described (Tosteson et al., 1994).

Large Unilamellar Vesicles

LUVs were prepared by extrusion from a 4:1:2 molar ratio of POPC:POPG: Cholesterol (Avanti Polar Lipids, Alabaster, AL) or a 4:1 molar ratio of POPC: POPG using purified wt M2 or M2 mutant protein where indicated.

Giant Unilamellar Vesicles

GUVs were electroformed using LUV lipid ratios with 0.5 mol % of TopFluor-Cholesterol (Avanti) added for visualization. Phase separated GUVs were electroformed at 60°C using a 2:2:1 or 10:10:1 molar ratio of DOPC:SM:Cholesterol, incorporating 0.5 mol % of TopFluor-Cholesterol and Rho-PE (Avanti). GUVs containing M2 protein were prepared through dehydration of M2-containing LUVs as previously described (Girard et al., 2004; Streicher et al., 2009).

Plasma Membrane Spheres

Plasma membrane spheres were prepared as previously described (Keller et al., 2009; Lingwood et al., 2008), transfected with M2 or M2(AH-Mut)-pCAGGS and incubated in PMS buffer for 12 hr. For visualization PMSs were incubated with labeled CTxB, stained for M2 and imaged at 37°C.

Budding Assay

293T cells were transfected with M2 or M2(AH-Mut)-pCAGGS. 24 hr post-transfection supernatant was collected and concentrated. Supernatant and cell lysates were analyzed by SDS-PAGE and immunoblotting as previously described (Chen et al., 2008).

SUPPLEMENTAL INFORMATION

Supplemental Information includes Extended Experimental Procedures, seven figures, and four movies and can be found with this article online at doi: 10.1016/j.cell.2010.08.029.

ACKNOWLEDGMENTS

We thank members of the Lamb laboratory for helpful discussions and critical reading of the manuscript. The electron microscopy was performed in the Northwestern University Biological Imaging Facility. This research was supported in part by a grant R01 AI-20201 from the National Institute of Allergy and Infectious Diseases. J.S.R. is an Associate and R.A.L. is an Investigator of the Howard Hughes Medical Institute.

Received: February 12, 2010
Revised: May 26, 2010
Accepted: August 5, 2010
Published: September 16, 2010

REFERENCES

Allain, J.M., and Ben Amar, M. (2006). Budding and fission of a multiphase vesicle. Eur. Phys. J. E *20*, 409–420.

Antonny, B. (2006). Membrane deformation by protein coats. Curr. Opin. Cell Biol. *18*, 386–394.

Barman, S., Adhikary, L., Chakrabarti, A.K., Bernas, C., Kawaoka, Y., and Nayak, D.P. (2004). Role of transmembrane domain and cytoplasmic tail amino acid sequences of influenza A virus neuraminidase in raft association and virus budding. J. Virol. *78*, 5258–5269.

Brown, D.A., and Rose, J.K. (1992). Sorting of GPI-anchored proteins to glycolipid-enriched membrane subdomains during transport to the apical cell surface. Cell *68*, 533–544.

Bruce, E.A., Digard, P., and Stuart, A.D. (2010). The rab11 pathway is required for influenza A virus budding and filament formation. J. Virol. *84*, 5848–5859.

Bruce, E.A., Medcalf, L., Crump, C.M., Noton, S.L., Stuart, A.D., Wise, H.M., Elton, D., Bowers, K., and Digard, P. (2009). Budding of filamentous and non-filamentous influenza A virus occurs via a VPS4 and VPS28-independent pathway. Virology *390*, 268–278.

Bui, M., Whittaker, G., and Helenius, A. (1996). Effect of M1 protein and low pH on nuclear transport of influenza virus ribonucleoproteins. J. Virol. *70*, 8391–8401.

Carlton, J.G., and Martin-Serrano, J. (2009). The ESCRT machinery: new functions in viral and cellular biology. Biochem. Soc. Trans. *37*, 195–199.

Chazal, N., and Gerlier, D. (2003). Virus entry, assembly, budding, and membrane rafts. Microbiol. Mol. Biol. Rev. *67*, 226–237.

Chen, B.J., and Lamb, R.A. (2008). Mechanisms for enveloped virus budding: can some viruses do without an ESCRT? Virology *372*, 221–232.

Chen, B.J., Leser, G.P., Jackson, D., and Lamb, R.A. (2008). The influenza virus M2 protein cytoplasmic tail interacts with the M1 protein and influences virus assembly at the site of virus budding. J. Virol. *82*, 10059–10070.

Chen, B.J., Leser, G.P., Morita, E., and Lamb, R.A. (2007). Influenza virus hemagglutinin and neuraminidase, but not the matrix protein, are required for assembly and budding of plasmid-derived virus-like particles. J. Virol. *81*, 7111–7123.

Chen, B.J., Takeda, M., and Lamb, R.A. (2005). Influenza virus hemagglutinin (H3 subtype) requires palmitoylation of its cytoplasmic tail for assembly: M1 proteins of two subtypes differ in their ability to support assembly. J. Virol. *79*, 13673–13684.

Chernomordik, L., Kozlov, M.M., and Zimmerberg, J. (1995). Lipids in biological membrane fusion. J. Membr. Biol. *146*, 1–14.

Cheung, T.K., Guan, Y., Ng, S.S., Chen, H., Wong, C.H., Peiris, J.S., and Poon, L.L. (2005). Generation of recombinant influenza A virus without M2 ion-channel protein by introduction of a point mutation at the 5′ end of the viral intron. J. Gen. Virol. *86*, 1447–1454.

de Meyer, F., and Smit, B. (2009). Effect of cholesterol on the structure of a phospholipid bilayer. Proc. Natl. Acad. Sci. USA *106*, 3654–3658.

Dempsey, C.E. (1990). The actions of melittin on membranes. Biochim. Biophys. Acta *1031*, 143–161.

Drin, G., and Antonny, B. (2010). Amphipathic helices and membrane curvature. FEBS Lett. *584*, 1840–1847.

Egashira, M., Gorbenko, G., Tanaka, M., Saito, H., Molotkovsky, J., Nakano, M., and Handa, T. (2002). Cholesterol modulates interaction between an amphipathic class A peptide, Ac-18A-NH2, and phosphatidylcholine bilayers. Biochemistry *41*, 4165–4172.

Girard, P., Pecreaux, J., Lenoir, G., Falson, P., Rigaud, J.L., and Bassereau, P. (2004). A new method for the reconstitution of membrane proteins into giant unilamellar vesicles. Biophys. J. *87*, 419–429.

Iwatsuki-Horimoto, K., Horimoto, T., Noda, T., Kiso, M., Maeda, J., Watanabe, S., Muramoto, Y., Fujii, K., and Kawaoka, Y. (2006). The cytoplasmic tail of the influenza A virus M2 protein plays a role in viral assembly. J. Virol. *80*, 5233–5240.

Jackson, D., and Lamb, R.A. (2008). The influenza A virus spliced messenger RNA M mRNA3 is not required for viral replication in tissue culture. J. Gen. Virol. *89*, 3097–3101.

Jin, H., Leser, G.P., Zhang, J., and Lamb, R.A. (1997). Influenza virus hemagglutinin and neuraminidase cytoplasmic tails control particle shape. EMBO J. *16*, 1236–1247.

Kaiser, H.J., Lingwood, D., Levental, I., Sampaio, J.L., Kalvodova, L., Rajendran, L., and Simons, K. (2009). Order of lipid phases in model and plasma membranes. Proc. Natl. Acad. Sci. USA *106*, 16645–16650.

Keller, H., Lorizate, M., and Schwille, P. (2009). PI(4,5)P2 degradation promotes the formation of cytoskeleton-free model membrane systems. ChemPhysChem *10*, 2805–2812.

Lamaziere, A., Burlina, F., Wolf, C., Chassaing, G., Trugnan, G., and Ayala-Sanmartin, J. (2007). Non-metabolic membrane tubulation and permeability induced by bioactive peptides. PLoS ONE *2*, e201.

Lamb, R.A., and Pinto, L.H. (2005). The proton selective ion channels of influenza A and B viruses. In Contemporary Topics in Influenza Virology, Y. Kawaoka, ed. (Wymondham, Norfolk, UK: Horizon Scientific Press), pp. 65–93.

Lee, M.T., Hung, W.C., Chen, F.Y., and Huang, H.W. (2008). Mechanism and kinetics of pore formation in membranes by water-soluble amphipathic peptides. Proc. Natl. Acad. Sci. USA *105*, 5087–5092.

Leser, G.P., Ector, K.J., and Lamb, R.A. (1996). The paramyxovirus simian virus 5 hemagglutinin-neuraminidase glycoprotein, but not the fusion glycoprotein, is internalized via coated pits and enters the endocytic pathway. Mol. Biol. Cell *7*, 155–172.

Leser, G.P., and Lamb, R.A. (2005). Influenza virus assembly and budding in raft-derived microdomains: a quantitative analysis of the surface distribution of HA, NA and M2 proteins. Virology *342*, 215–227.

Lingwood, D., Ries, J., Schwille, P., and Simons, K. (2008). Plasma membranes are poised for activation of raft phase coalescence at physiological temperature. Proc. Natl. Acad. Sci. USA *105*, 10005–10010.

Liu, J., Kaksonen, M., Drubin, D.G., and Oster, G. (2006). Endocytic vesicle scission by lipid phase boundary forces. Proc. Natl. Acad. Sci. USA *103*, 10277–10282.

Ma, C., Polishchuk, A.L., Ohigashi, Y., Stouffer, A.L., Schon, A., Magavern, E., Jing, X., Lear, J.D., Freire, E., Lamb, R.A., et al. (2009). Identification of the functional core of the influenza A virus A/M2 proton-selective ion channel. Proc. Natl. Acad. Sci. USA *106*, 12283–12288.

McCown, M.F., and Pekosz, A. (2005). The influenza A virus M2 cytoplasmic tail is required for infectious virus production and efficient genome packaging. J. Virol. *79*, 3595–3605.

McCown, M.F., and Pekosz, A. (2006). Distinct domains of the influenza A virus M2 protein cytoplasmic tail mediate binding to the M1 protein and facilitate infectious virus production. J. Virol. *80*, 8178–8189.

Nguyen, P.A., Soto, C.S., Polishchuk, A., Caputo, G.A., Tatko, C.D., Ma, C., Ohigashi, Y., Pinto, L.H., DeGrado, W.F., and Howard, K.P. (2008). pH-induced conformational change of the influenza M2 protein C-terminal domain. Biochemistry *47*, 9934–9936.

Noton, S.L., Medcalf, E., Fisher, D., Mullin, A.E., Elton, D., and Digard, P. (2007). Identification of the domains of the influenza A virus M1 matrix protein required for NP binding, oligomerization and incorporation into virions. J. Gen. Virol. *88*, 2280–2290.

Pattnaik, A.K., Brown, D.J., and Nayak, D.P. (1986). Formation of influenza virus particles lacking hemagglutinin on the viral envelope. J. Virol. *60*, 994–1001.

Pinto, L.H., Dieckmann, G.R., Gandhi, C.S., Papworth, C.G., Braman, J., Shaughnessy, M.A., Lear, J.D., Lamb, R.A., and DeGrado, W.F. (1997). A functionally defined model for the M_2 proton channel of influenza A virus suggests a mechanism for its ion selectivity. Proc. Natl. Acad. Sci. USA *94*, 11301–11306.

Pinto, L.H., and Lamb, R.A. (2006). The M2 proton channels of influenza A and B viruses. J. Biol. Chem. *281*, 8997–9000.

Pinto, L.H., and Lamb, R.A. (2007). Controlling influenza virus replication by inhibiting its proton channel. Mol. Biosyst. *3*, 18–23.

Romer, W., Pontani, L.L., Sorre, B., Rentero, C., Berland, L., Chambon, V., Lamaze, C., Bassereau, P., Sykes, C., Gaus, K., et al. (2010). Actin dynamics drive membrane reorganization and scission in clathrin-independent endocytosis. Cell *140*, 540–553.

Rossman, J.S., Jing, X., Leser, G.P., Balannik, V., Pinto, L.H., and Lamb, R.A. (2010). Influenza virus M2 ion channel protein is necessary for filamentous virion formation. J. Virol. *84*, 5078–5088.

Russell, C.J., Jardetzky, T.S., and Lamb, R.A. (2001). Membrane fusion machines of paramyxoviruses: capture of intermediates of fusion. EMBO J. *20*, 4024–4034.

Schnell, J.R., and Chou, J.J. (2008). Structure and mechanism of the M2 proton channel of influenza A virus. Nature *451*, 591–595.

Schroeder, C., Heider, H., Moncke-Buchner, E., and Lin, T.I. (2005). The influenza virus ion channel and maturation cofactor M2 is a cholesterol-binding protein. Eur. Biophys. J. *34*, 52–66.

Simons, K., and Toomre, D. (2000). Lipid rafts and signal transduction. Nat. Rev. Mol. Cell Biol. *1*, 31–39.

Streicher, P., Nassoy, P., Barmann, M., Dif, A., Marchi-Artzner, V., Brochard-Wyart, F., Spatz, J., and Bassereau, P. (2009). Integrin reconstituted in GUVs: a biomimetic system to study initial steps of cell spreading. Biochim. Biophys. Acta *1788*, 2291–2300.

Takeda, M., Leser, G.P., Russell, C.J., and Lamb, R.A. (2003). Influenza virus hemagglutinin concentrates in lipid raft microdomains for efficient viral fusion. Proc. Natl. Acad. Sci. USA *100*, 14610–14617.

Tian, C., Gao, P.F., Pinto, L.H., Lamb, R.A., and Cross, T.A. (2003). Initial structural and dynamic characterization of the M2 protein transmembrane and amphipathic helices in lipid bilayers. Protein Sci. *12*, 2597–2605.

Tosteson, M.T., Pinto, L.H., Holsinger, L.J., and Lamb, R.A. (1994). Reconstitution of the influenza virus M_2 ion channel in lipid bilayers. J. Membr. Biol. *142*, 117–126.

Venkatachalapathi, Y.V., Phillips, M.C., Epand, R.M., Epand, R.F., Tytler, E.M., Segrest, J.P., and Anantharamaiah, G.M. (1993). Effect of end group blockage on the properties of a class A amphipathic helical peptide. Proteins *15*, 349–359.

Wollert, T., Wunder, C., Lippincott-Schwartz, J., and Hurley, J.H. (2009). Membrane scission by the ESCRT-III complex. Nature *458*, 172–177.

Yuan, B., Campbell, S., Bacharach, E., Rein, A., and Goff, S.P. (2000). Infectivity of Moloney murine leukemia virus defective in late assembly events is restored by late assembly domains of other retroviruses. J. Virol. *74*, 7250–7260.

Zebedee, S.L., and Lamb, R.A. (1988). Influenza A virus M_2 protein: monoclonal antibody restriction of virus growth and detection of M_2 in virions. J. Virol. *62*, 2762–2772.

Zhang, J., and Lamb, R.A. (1996). Characterization of the membrane association of the influenza virus matrix protein in living cells. Virology *225*, 255–266.

Cell

EXTENDED EXPERIMENTAL PROCEDURES

Cell, Viruses, and Reagents

Madin-Darby canine kidney (MDCK) cells, M2-MDCK cells, 293T cells, viral stock propagation and viral infections were as previously described (Chen et al., 2008). A549 and A431 cells were from ATCC (Manassas, VA). M2 AH-Mut (previously called M2-Helix) and ΔM2 recombinant viruses have been previously described (Rossman et al., 2010; Jackson and Lamb, 2008). Antibodies used were: αHA (NR3118, BEI, Manassas, VA), αM2 (ectodomain mAbs 14C2 and 5C4; (Zebedee and Lamb, 1988), αRab11a (Invitrogen, Carlsbad, CA), αTubulin (Invitrogen) Alexa-488 and Alexa-594 fluorophore-conjugated secondary antibodies (Invitrogen) and a 6 nm gold conjugated secondary antibody (Jackson ImmunoResearch, West Grove, PA). Peptides were synthesized and purified by GenScript (Piscataway, NJ) to > 90% purity. All peptides except RW16 and melittin were modified by N-terminal acetylation and C-terminal amidation. Peptide sources and sequences used were: M2AH, from A/Udorn/72 LFFKCIYRFFEHGLKRG; M2AH-Mut, from A/Udorn/72 M2 AH-Mut, LAAKCAARFAEHGLKRG; M2AH-WSN, from A/WSN/33, LFFKCIYRRFKYGLKRG; M2AH-SOIV, from A/California/05/2009, LFFKCIYRRFKYGLKRG, which matches the consensus sequence for all 2009 H1N1 swine-origin influenza virus strains; M2AH-Scrambled, created from 51 iterations of random reordering of A/Udorn/72 M2AH sequence, FFKLGYLEFKIFRGCRH; Ac-18A-NH2 from (Venkatachalapathi et al., 1993), DWLKAFYDKVAEKLKEAF; RW16 from (Lamaziere et al., 2007), RRWRRWWRRWWRRWRR; Melittin from honey bee venom, GIGAVLKVLTTGLPALISWIKRKRQQ-NH2.

Immunofluorescence Microscopy

MDCK cells grown on glass coverslips were infected as indicated, fixed in 10% formalin:PBS (Electron Microscopy Sciences, Hatsfield, PA) and stained for HA and M2 without permeabilization. For examination of M2 localization on budded viral filaments, virus supernatant was spotted on a glass coverslip for 1 hr at 4°C, fixed and stained as above. For quantification, a minimum of 100 filaments were counted and examined for M2 foci from 7 different images with average and standard deviation calculated for the percentage of filaments containing an M2 focus. For examination of the effect of Rab11 knock-down, A549 cells grown on glass coverslips were transfected with control siRNA (siGlo, Dharmacon, Lafayette, CO) or a combination of siRNAs targeting Rab11a and Rab11b (siGENOME SMARTpool, Dharmacon) using Dharmafect 1 reagent, giving a final total siRNA concentration of 0.1μM. 48 hr post-transfection cells were infected with a MOI of 3 pfu/cell of A/Udorn/72 for 18 hr, fixed and stained for HA and M2 with and without permeabilization. Imaging parameters were adjusted for control samples and held constant for imaging of the respective Rab11 knock-down sample. No manipulation of image levels was performed. Fluorescent intensity was quantified for a minimum of 50 cells and averaged.

Images were collected on a LSM5 Pascal (Zeiss, Thornwood, NY) confocal microscope using a 63x Plan-Apochromat objective (Zeiss) in multitrack mode. Alexa-488 samples were imaged using the 488 nm line of an argon laser (Lasos, Jena, Germany), a 488/543/633 nm excitation filter, a 545 nm dichroic and a 505-530 nm emission filter. Alexa-594 samples were imaged using a 594 nm HeNe laser line (Lasos), a 488/543/633 nm excitation filter, a 545 nm dichroic and a 560 nm emission filter. For GUV imaging, the Lo marker TopFluor-Cholesterol (Avanti) was imaged using the 488nm line of an argon laser (Lasos), a 488/543/633 nm excitation filter, a 545 nm dichroic and a 505-530 nm emission filter. The Ld marker 18:1 lissamine-rhodamine-PE (Avanti) was imaged using a 543 nm HeNe laser line (Lasos), a 488/543/633 nm excitation filter, a 545 nm dichroic and a 560 nm emission filter. Tetramethylrhodamine-labeled M2AH peptide was imaged using the above setting for Rho-PE. Lucifer yellow (Invitrogen) was imaged using the 458 nm line of an argon laser (Lasos), a 458/543/633 nm excitation filter, a 545 nm dichroic and a 560 nm emission filter. Settings were optimized to eliminate crosstalk between detection channels. Post-imaging manipulation was performed in Photoshop (Adobe, San Jose, CA) and was limited to image cropping and even adjustments of image levels across the entire image.

Electron Microscopy

LUV preparations were treated as indicated and absorbed to glow-discharge treated (208C High Vacuum Turbo Carbon Coater, Ted Pella, Redding, CA) carbon-formvar coated, 300 mesh copper grids (Electron Microscopy Sciences) and stained with 2% phosphotungstic acid for 30 s before imaging. For cryo-electron microscopy, LUV preparations were absorbed to glow-discharge treated carbon-formvar 200 mesh copper grids (Electron Microscopy Sciences) and imbedded in vitreous ice using an FEI Vitrobot Mark IV (Hillsboro, Or) at room temperature and 100% humidity. Samples were imaged using a Gatan (Pleasanton, CA) cryo-holder operating at −180°C. For analysis of virus-infected cells, MDCK cells were treated as indicated and subjected to preembedding αM2 immunogold labeling followed by thin section examination as previously described (Leser et al., 1996). For M2 detection by immunogold labeling it was found to be necessary to utilize 6nm gold-conjugated secondary antibodies, as larger gold conjugates gave lower labeling densities, possibly due to steric interference following binding to the short ectodomain of M2. Samples were imaged on a JEOL 1230 electron microscope (JEOL, Tokyo, Japan) at 100 keV. Images were captured using a Gatan digital camera. Post-imaging manipulation was performed in Photoshop (Adobe) and was limited to image cropping and equal adjustment of image levels and contrast. M2 localization was quantified by counting the number of gold particles found at the neck of budding virions compared to the total number of gold particles on the image for over 50 section images, or the number of gold particles at one foci on budded virions compared to the total number of gold particles on the virion for over 50 virions.

Protein Purification

M2 and M2(AH-Mut) were expressed using the Bac-N-Blue baculovirus expression system (Invitrogen) in Sf9 cells. Protein purification was performed as previously described (Tosteson et al., 1994). In brief: 48 hr p. i. baculovirus-infected Sf9 cells were pelleted, resuspended in the presence of protease inhibitors and disrupted using 20 strokes of a Dounce homogenizer. Membrane-associated M2 was separated from bulk cell lysate by ultracentrifugation through 30 and 60% sucrose using a SW28 rotor (Beckman, Fullerton, CA) at 22,000 rpm for 16 hr at 4°C. Protein at the 30%–60% sucrose interface was collected and the sucrose removed by dialysis, using a 3.5 kDa molecular weight cut-off membrane (Pierce, Rockford, IL). Protein was resuspended in 33 mM octylglucoside and separated from insoluble membrane by centrifugation using a Ti70 rotor (Beckman) at 37,000 rpm for 30 min at 4°C. Supernatant was flowed over a mAb-14C2 conjugated Sepharose column (CNBr activated Sepharose, Pharmacia, Piscataway, NJ), washed and eluted. Protein was washed, concentrated and buffer exchanged into 50 mM Tris pH7.4, 20% glycerol, 4 mM octylglucoside using an Amicon Ultra 3,000 MW cut-off filter (Millipore, Billerica, MA). Protein purity was assessed by SDS-PAGE and silver stain plus (Bio-Rad, Hercules, CA) and protein concentration was determined by BCA assay (Pierce).

Large Unilamellar Vesicles

LUVs were prepared from a 4:1:2 molar ratio of POPC:POPG:Cholesterol (Avanti Polar Lipids, Alabaster, AL), a 4:1:1 molar ratio or a 4:1 molar ratio of POPC:POPG using 12.5 μmole of total lipid in each experiment. Lipid solutions were mixed, dried under argon gas and lyophilized in a FreezeZone 2.5plus lyophilizer (Labconco, Kansas City, MO). Lipid films were reconstituted in K buffer (10 mM K_2HPO_4, 50 mM K_2SO_4, 5 mM MOPS pH 7.4, 40 mM octylglucoside) and mixed where indicated with 100 μg of purified wt M2 or M2 mutant protein (in 50 mM Tris pH 7.4, 20% glycerol, 4 mM octylglucoside) and diluted with ddH_20 until the concentration of octylglucoside dropped below the critical micelle concentration of 25 mM, yielding a final molar % of protein equal to 0.048% and a final mass % equal to 1.09%. As M2 and M2(AH-Mut) proteins contain intact transmembrane domains, protein incorporation into LUVs required 15 cycles of freeze-thaw. LUVs were then extruded 21 times through a 100 nm polycarbonate membrane using an Avanti extruder (Avanti), treated as indicated and prepared for transmission electron microscopy as indicated. To test for protein incorporation, LUVs were separated from supernatant by passage through an Amicon Ultra 100,000 MW cut-off filter (Millipore) and the unincorporated protein was quantified with the Pierce BCA assay kit.

Giant Unilamellar Vesicles

GUVs were prepared from a 1 mg/ml solution of lipids in chloroform, containing either a 4:1:2 molar ratio of POPC:POPG:Cholesterol (Avanti), a 4:1:1 molar ratio or a 4:1 molar ratio of POPC:POPG. For visualization of the GUVs by light microscopy, 0.5 mol % of TopFluor-Cholesterol (Avanti) was added to the lipid solutions. 6.4 μl of the lipid solution was then evaporated onto the conductive side of each of two indium-tin oxide coated slides (70-100 Ω, Delta Technologies, Stillwater, MN), onto a 6.4 cm^2 area and dehydrated under vacuum for 1 hr. After dehydration, electroformation chambers were constructed by sandwiching a FastWell 9 mm spacer (Grace Bio Labs, Bend, OR) between two lipid-coated coverslips. The lipids were rehydrated with 0.1 M sucrose, 1 mM HEPES, pH 7.2 and a 10 Hz sine wave of 1 V was applied across the chamber for 4 hr using a function generator (GW Instek, Taipei, Taiwan). Phase-separated GUVs were prepared as above using either a 2:2:1 or a 10:10:1 molar ratio of DOPC:SM:Cholesterol (Avanti) incorporating 0.5 mol % of TopFluor-Cholesterol and 0.5 mol % of Liss-Rho-PE. Electroformation was carried out at 60°C for 4 hr, after which the GUVs were immediately cooled to room temperature.

GUVs containing M2 protein were prepared through dehydration of M2-containing LUVs as previously described (Girard et al., 2004; Streicher et al., 2009). M2 and M2(AH-Mut) containing LUVs were prepared as above with the addition of 0.5 mol % of TopFluor-Cholesterol (Avanti). Following extrusion, LUVs were diluted 1:10 in K buffer and 12.8 μl was dehydrated onto indium-tin oxide coated slides (Delta Technologies) as described above for 2 hr under the saturated vapor pressure of a saturated NaCl solution. The lipids were rehydrated and electroformed as above for 16 hr. To detach the GUVs from the slides a 4 Hz square wave of 2 V was applied across the chamber for 1 hr using a function generator (GW Instek).

GUVs were then harvested using a wide-bore pipette tip and diluted 1:100 (1:10 for protein containing GUVs) in resuspension buffer (0.1 M glucose, 1 mM HEPES, pH. 7.2) and allowed to settle for 30 min before use. GUVs were imaged in Nunc Lab-Tek II chamber slides (Thermo Fisher Scientific, Rochester, NY) that had been blocked with 5% milk for 1 hr before use. All GUVs were imaged within 4 hr of electroformation. Where indicated, 0.5 mg/ml Lucifer yellow (Invitrogen) was added to the GUV resuspension and imaging buffer. Where indicated during continuous GUV imaging, an equal volume of dilution buffer was added containing 20 μM of the indicated peptide (to give a final peptide concentration of 10 μM). Quantification of GUV budding was performed by determining the percentage of GUVs containing at least one ILV and the percentage of GUVs containing at least one lucifer yellow positive ILV for at least 40 GUVs.

Plasma Membrane Spheres

Plasma membrane spheres were prepared as previously described (Keller et al., 2009; Lingwood et al., 2008). Briefly, A431 cells were seeded on poly-D-lysine coated glass bottom dishes (MatTek, Ashland, MA). 24 hr later cells were transfected with M2-pCAGGS or M2(AH-Mut)-pCAGGS using Lipofectamine 2000 (Invitrogen). 24 hr post-transfection cells were washed and incubated for 12 hr in PMS buffer (1.5 mM $CaCl_2$, 1.5 mM $MgCl_2$, 5 mM HEPES pH 7.4, 1 mg/ml glucose in 1x PBS) at 37°C. The lipid ordered phase was visualized through GM1 crosslinking by incubating the PMS in 10μg/ml of Alexa-488 labeled cholera-toxin subunit B (Invitrogen) for

2 hr at 37°C. M2 was visualized by immunofluorescent staining, incubating the PMS with the αM2-ectodomain antibody, 5C4, and an Alexa-594 labeled secondary antibody, for 1 hr each at 37°C. PMS were then washed and imaged at 37°C with 5% CO_2 using the Zeiss Incubator S system.

Budding Assay

6 cm dishes of 293T cells were transfected with 8 μg of M2-pCAGGS or M2(AH-Mut)-pCAGGS, or 2 μg of M2-pCAGGS for reduced M2 expression, using Lipofectamine 2000 (Invitrogen). 24 hr post-transfection supernatant was collected and concentrated 10-fold in an Amicon Ultra 10,000 MW cut-off filter (Millipore). Cells were lysed in 1x RIPA buffer (1% deoxycholic acid, 1% TX-100, 0.1% sodium dodecyl sulfate, 10 mM Tris pH 7.4, 0.3 M NaCl) with 1x complete protease inhibitor cocktail (Roche, Basel, Switzerland) for 30 min at 4°C. Insoluble material was pelleted by centrifugation at 14,000 x g at 4°C for 10 min. Supernatant and cell lysates were analyzed by SDS-PAGE and immunoblotting as previously described (Chen et al., 2008), with band intensities quantified in Photoshop (Adobe).

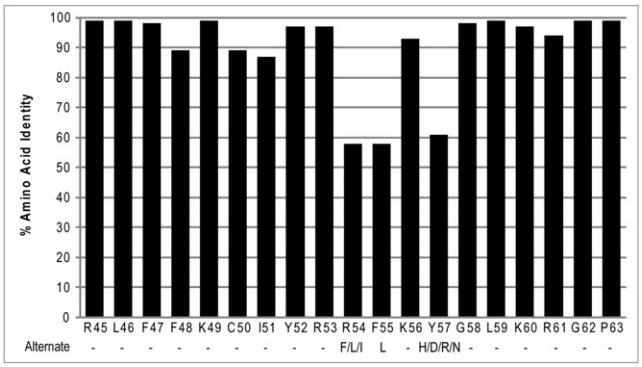

Figure S1. Conservation of the M2 Amphipathic Helix, Related to Figure 1

Alignment of 500 influenza A virus M2 protein sequences covering multiple subtypes, hosts and isolate years. The alignment was created at http://www.ncbi.nlm.nih.gov/genomes/FLU and is displayed as % amino acid identity to the averaged consensus sequence shown below. Alternate amino acids are listed for positions exhibiting less than 85% identity.

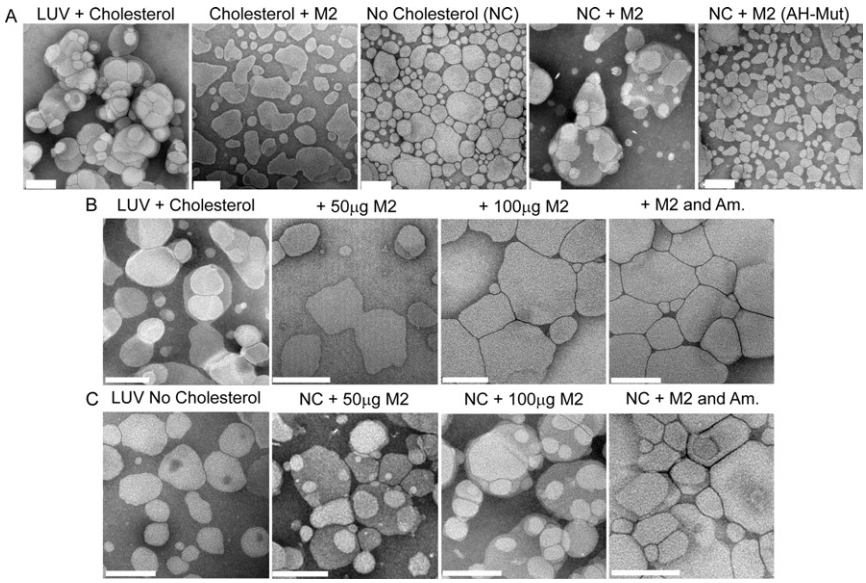

Figure S2. M2 Alteration of Membrane Curvature Does Not Depend on Ion Channel Activity, Related to Figure 2

(A) LUVs were prepared as in Figure 2A and analyzed by negative staining and electron microscopy. (B) LUVs or (C) cholesterol-free LUVs were prepared as above with 50 or 100 μg of M2 protein where indicated and treated with 100 μM amantadine for one hour at 37° C where indicated before examination by electron microscopy. Scale bars indicate 100 nm.

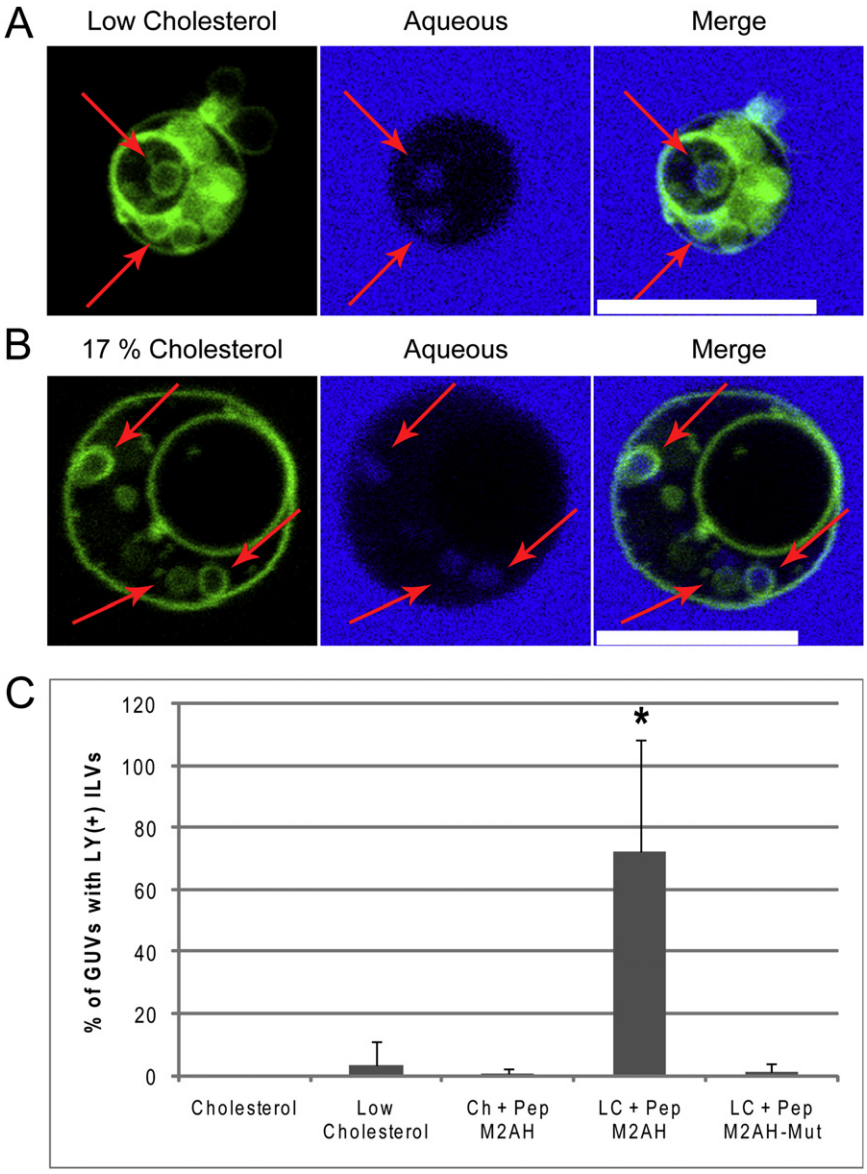

Figure S3. M2-Mediated Uptake of Aqueous Media, Related to Figures 2 and 3

(A) Low-cholesterol and (B) 17 molar % cholesterol, M2-containing, GUV images from Figure 2 enlarged for clarity. The membrane is shown in green and the lucifer yellow aqueous phase is shown in blue. Arrows indicate lucifer yellow containing ILVs. Scale bars indicate 10 μm. (C) Quantification of M2AH peptide-induced budding. The percentage of GUVs containing at least one lucifer yellow-positive ILV were averaged over multiple images for a minimum of three separate experiments and included a minimum of 40 GUVs. Bars indicate averages ± standard deviation. * Indicates a significant difference from untreated GUVs as determined by the student's t test, $p < 0.0001$.

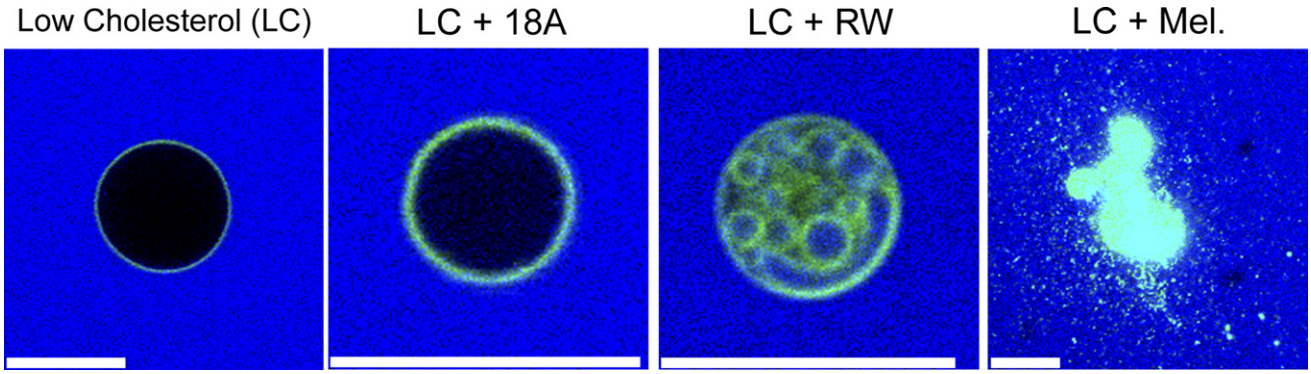

Figure S4. Amphipathic Peptides Exert Different Effects on GUV Membranes, Related to Figure 3

Low-cholesterol GUVs, prepared as for Figure 3B, were treated with 10 μM of the indicated peptide for 1 hr and imaged. 18A corresponds to the peptide Ac-18A-NH2, RW to the peptide RW16 and Mel to the peptide melittin. Scale bars indicate 10 μm.

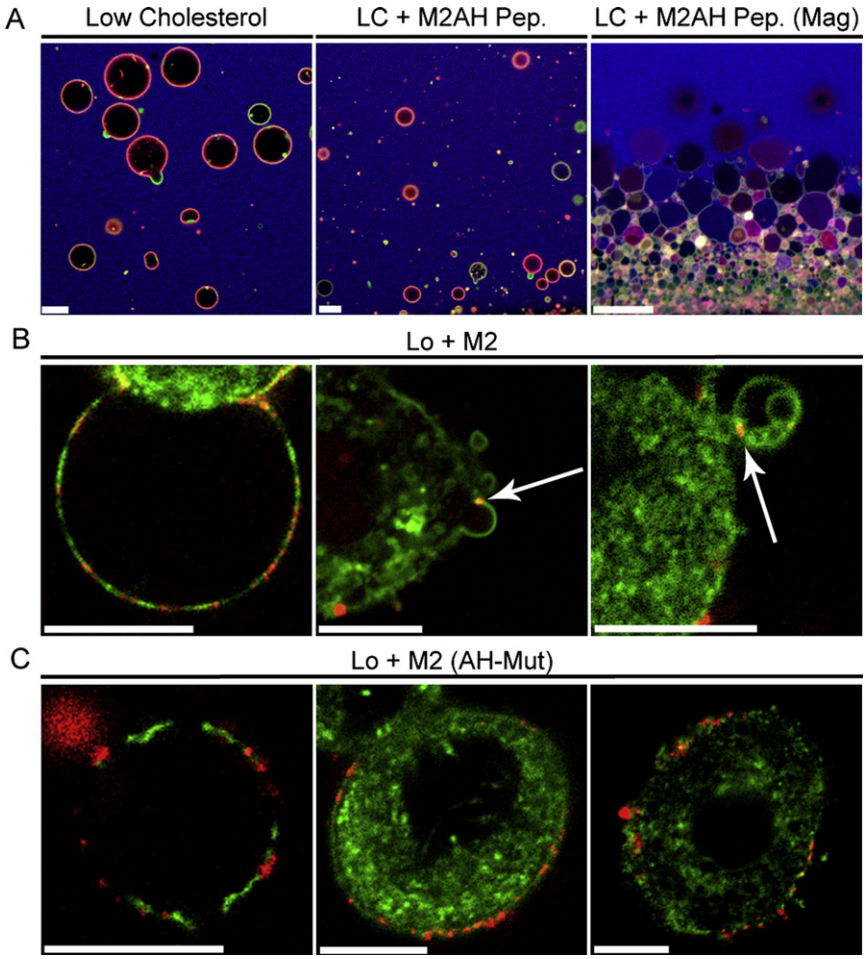

Figure S5. The M2 Amphipathic Helix Causes Budding of Low-Cholesterol Phase-Separated GUVs, Related to Figure 4

(A) Additional images of low-cholesterol, phase-separated, GUVs treated with 10μM M2AH peptide for 1 hr as shown in Figure 4D. Mag indicates a higher magnification image of M2AH-treated GUVs seen at the chamber edge where small, budded, GUVs have accumulated. The Lo phase is shown in green, the Ld phase in red and the aqueous media is shown in blue. (B) Additional images of, M2-expressing, plasma membrane spheres from Figure 4G, showing phase-segregation of M2 and the formation of budding vesicles at the boundary between M2 and the Lo phase (indicated by arrows). (C) Additional images of M2 (AH-Mut)-expressing plasma membrane spheres from Figure 4G. The Lo phase is shown in green and M2 is shown in red. Scale bars indicate 10 μm.

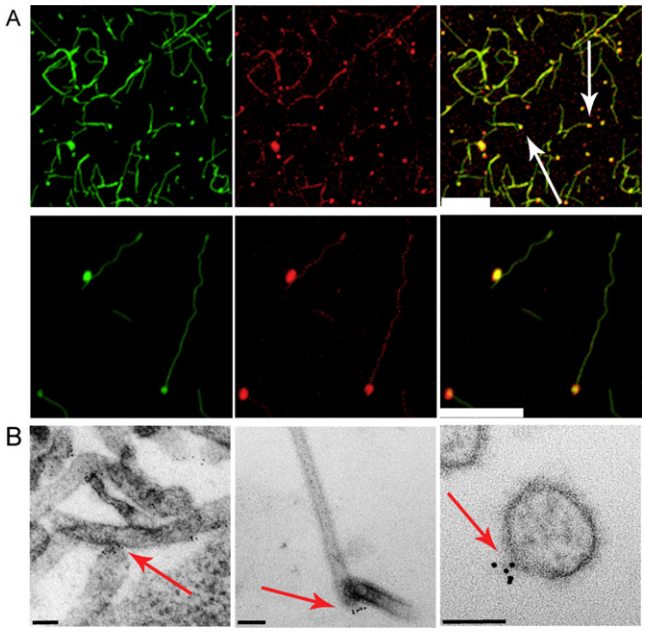

Figure S6. M2 Localization on Budded Virions, Related to Figure 6

(A) MDCK cells were infected with an MOI of 0.001 pfu/cell of A/Udorn/72 for 48 hr, virus-containing supernatant was harvested, clarified, spotted on a glass coverslip, fixed and stained for HA (shown in green) and M2 (shown in red). Lower panel is a magnification of images shown in Figure S6a. Scale bars indicate 10 μm. Levels (red-channel) were increased in Photoshop to better show the faint M2 localization along the length of the filament. (B) MDCK cells were infected with an MOI of 3 pfu/cell of A/Udorn/72 for 18 hr, stained for M2 via immunogold labeling and thin sections were analyzed by electron microscopy. Scale bars indicate 100 nm. Arrows indicate foci of M2.

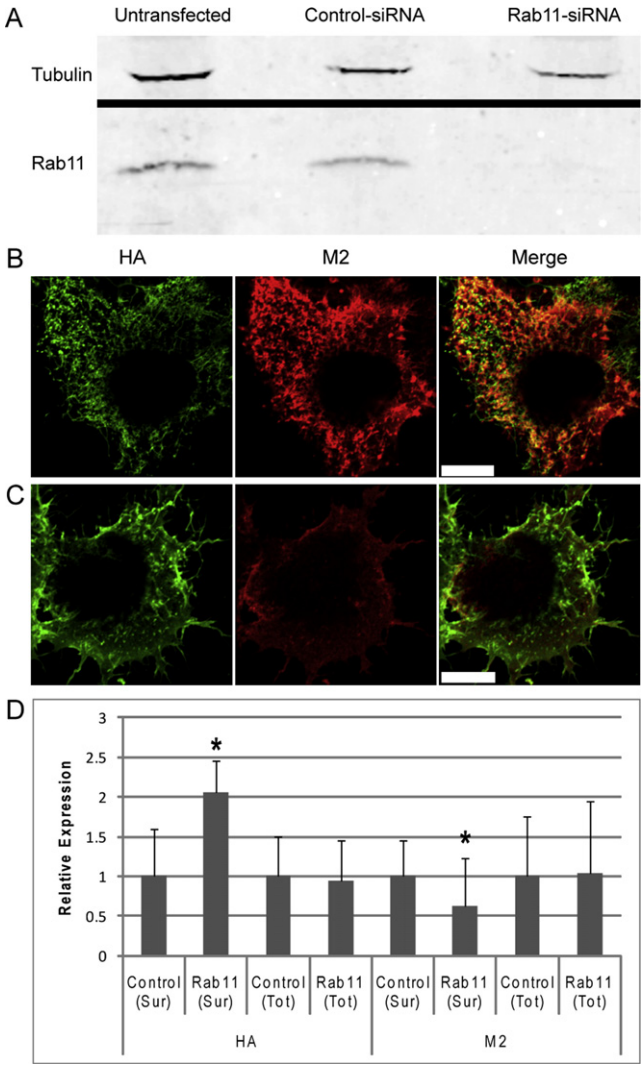

Figure S7. Rab11 Knock-down Alters M2 Surface Expression

(A) A549 cells were transfected with a control siRNA or siRNAs targeting Rab11a and Rab11b. 48 hr. post-transfection, cells were lysed and Rab11a expression was determined by Western blot as compared to a tubulin loading control. Bar indicates separate images. (B) 48 hr. post-transfection, control siRNA transfected cells or (C) Rab11a/b siRNA transfected cells were infected with influenza virus at an MOI of 3 pfu/cell for 18 hr. Cells were stained for HA and M2. Scale bars indicate 10 μm. (D) Quantification of the surface expression (Sur), and total expression (Tot), as measured by immunofluorescent staining following permeabilization of the cells, of HA and M2 from a minimum of 50 control and siRNA treated cells, with the control-treated levels of HA and M2 set as 100%. Bars indicate averages ± standard deviation. * Indicates a significant difference from control-treated cells as determined by the student's t test, with p-values of < 0.001, all other pairwise comparisons to control samples were not significant with p-values of > 0.4.